

**UNCLASSIFIED**

**AD 415 157**

**DEFENSE DOCUMENTATION CENTER**

**FOR**

**SCIENTIFIC AND TECHNICAL INFORMATION**

**CAMERON STATION, ALEXANDRIA, VIRGINIA**



**UNCLASSIFIED**

NOTICE: When government or other drawings, specifications or other data are used for any purpose other than in connection with a definitely related government procurement operation, the U. S. Government thereby incurs no responsibility, nor any obligation whatsoever; and the fact that the Government may have formulated, furnished, or in any way supplied the said drawings, specifications, or other data is not to be regarded by implication or otherwise as in any manner licensing the holder or any other person or corporation, or conveying any rights or permission to manufacture, use or sell any patented invention that may in any way be related thereto.

63-4-5

415157

CATALOGED BY DDC  
AS AD No. 415157

Fourth Interim Report  
FEASIBILITY STUDIES OF  
POYNTING VECTOR MEASUREMENTS

A report of research work for the period  
1 April to 30 June 1963  
Under Contract NBy-32219

DDC  
RECEIVED  
AUG 31 1963  
JISIA E

Serial No. \_\_\_\_\_

Fourth Interim Report  
FEASIBILITY STUDIES OF  
POYNTING VECTOR MEASUREMENTS

A report of research work for the period  
1 April to 30 June 1963  
Under Contract NBy-32219

between

U. S. Naval Civil Engineering Laboratory  
Port Hueneme, California

and

University of Pennsylvania  
The Moore School of Electrical Engineering  
Philadelphia, Pennsylvania

This report was prepared by:

R. A. Bartfeld  
R. G. Milholland  
P. B. Swarup

31 July 1963

Moore School Report No. 63-23

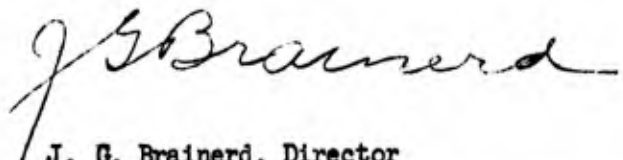
The following members of the Communications Section, Moore School of Electrical Engineering, contributed to the work reported herein:

Robert A. Bartfeld  
Robert G. Mulholland  
Pande B. Swarup  
Ralph M. Showers

Approved:



R. M. Showers, Section Head  
Moore School of Electrical Engineering



J. G. Brainerd, Director  
Moore School of Electrical Engineering

## TABLE OF CONTENTS

	<u>Page</u>
List of Figures .....	v
Abstract .....	vi
Summary .....	vii
1. THE PRINCIPLE OF POYNTING VECTOR MEASUREMENTS .....	1
1.1 Introduction .....	1
1.2 The Poynting Vector .....	1
1.3 The Electric Point Source .....	3
1.3.1 Associated Impedances and Phase .....	5
1.3.2 Associated Power Flow .....	7
1.4 The Magnetic Point Source .....	10
1.4.1 Associated Impedances and Phase .....	11
1.4.2 Associated Power Flow .....	12
2. THEORETICAL CONSIDERATIONS .....	13
2.1 Introduction .....	13
2.2 Interaction Errors of the Poynting Sensor .....	14
2.3 Interaction Errors in the Presence of a Short Dipole Transmitting Antenna .....	18
2.4 Remarks on the Impedance Concept .....	20
3. NEAR FIELD MEASUREMENTS OF ELECTRIC AND MAGNETIC FIELD COMPONENTS .....	21
3.1 Introduction .....	21
3.2 Practical Near-Field Sensors .....	21
3.3 The Image Plane and its Sensors .....	23
3.4 The Instrument Setup .....	26
4. POWER AND PHASE MEASUREMENTS IN THE NEAR FIELD .....	30
4.1 Introduction .....	30
4.2 The Poynting Sensor .....	30
4.3 The Instrument Setup .....	32
4.4 Phase Measurements .....	34
4.5 Summary and Conclusions .....	47
Appendix A INTERNAL RESISTANCE OF CYLINDRICAL DIPOLE ANTENNA .....	48
A.1 Introduction .....	48
A.2 Calculation of Internal Impedance .....	48

	<u>Page</u>
A.3 Comparison of Internal and Radiation Resistances	50
A.4 Conclusion .....	54
Appendix B INFLUENCE OF GAP ON DIPOLE INPUT IMPEDANCE .....	55
B.1 Introduction .....	55
B.2 Influence of the Gap Width in a Spheroidal Model	55
B.3 Influence of the Gap Width on Hallen Model .....	59
B.4 Analysis and Conclusion .....	64
References .....	67

## LIST OF FIGURES

<u>Figure No.</u>	<u>Page</u>
1.3.1 The Electric Dipole .....	3
1.4.1 The Magnetic Dipole .....	11
2.2.1 Poynting Sensor and Transmitting Antenna .....	14
3.3.1 Dipole-Dipole Measurements .....	24
3.3.2 Principle of Operation of Semicircular Loop .....	25
3.3.3 Radiation Pattern of a Semicircular Loop .....	27
3.3.4 Loop-Dipole Measurements .....	28
3.3.5 Loop-Loop Measurements .....	29
4.3.1 Block Diagram for Phase Measurements .....	33
4.3.2 Vector Diagram for Phase Measurements .....	33
4.4.1 Poynting Sensor in Vicinity of Electric Source .....	35
4.4.2 Poynting Sensor in Vicinity of Magnetic Source .....	35
4.4.3 Phase Measurements of Electric Source $\gamma_0 = 90^\circ$ .....	38
4.4.4 Magnitude Measurements of Electric Source $\gamma_0 = 90^\circ$ ....	39
4.4.5 Phase Measurements of Electric Source $\gamma_0 = 48^\circ$ .....	41
4.4.6 Magnitude Measurements of Electric Source $\gamma_0 = 48^\circ$ ....	42
4.4.7 Phase Measurements of Electric Source $\gamma_0 = 56^\circ$ .....	43
4.4.8 Phase Measurements of Magnetic Source $\gamma_0 = 60^\circ$ .....	44
4.4.9 Magnitude Measurements of Magnetic Source $\gamma_0 = 60^\circ$ ....	45
4.4.10 $EH \cos \theta$ vs. Distance Electric Source .....	46
A.1 Radiating and Internal Resistances of Cylindrical Short Dipole .....	51
A.2 Input Resistances of the Center-Driven Dipole Antenna ..	52
A.3 Radiating and Internal Resistance of Cylindrical Dipole.	53
B.1 Input Resistance with Finite Gap .....	66



## FEASIBILITY STUDIES OF POYNTING VECTOR MEASUREMENTS

## ABSTRACT

Feasibility studies of Poynting vector measurements were undertaken as a result of previous studies concerning methods of improved measurements in the near field of radiating sources. In previous reports it was indicated that a new type of near field measurement, the Poynting vector measurement, has some distinct advantages over presently used methods. The present study concerns itself with the feasibility of those measurements and a demonstration of the principle involved.

## SUMMARY

An experimental setup was obtained that enabled measurements of near-field properties of radiating sources. The radiating sources, acting as electric and magnetic point sources, consisted of small monopole antennas and semicircular loops. Most measurements were conducted in the 100-300 Mc range. Using a Poynting sensor as the receiving element measurements of the electromagnetic field were performed as a function of distance from the source. The measurements included magnitude measurements of the E and H components and their relative time phase. Results agreed closely with predicted curves. In particular it was possible to obtain Poynting vector measurements in the near field and thus demonstrate, in principle, the feasibility of such measurements.

## 1. THE PRINCIPLE OF POYNTING VECTOR MEASUREMENTS

### 1.1 Introduction

The present chapter provides a background of the basic theoretical considerations underlying Poynting vector measurements. After a brief discussion of the Poynting vector itself the electromagnetic field components of electric and magnetic point sources are introduced. Their phase properties, associated impedances and the resulting power density are discussed from a theoretical point of view.

### 1.2 The Poynting Vector

Since most of this report concerns itself with the Poynting vector and its measurement it is desirable to start with a brief description of this concept.

The energy equation for an electromagnetic field can be obtained from Maxwell's equations

$$\nabla \times \mathbf{H} = \mathbf{J} + \frac{\partial \mathbf{D}}{\partial t} \quad (1.2.1)$$

$$\nabla \times \mathbf{E} = - \frac{\partial \mathbf{B}}{\partial t} \quad (1.2.2)$$

where

E - Electric field

H - Magnetic field

J - Current density

B - Magnetic induction

D - Electric displacement

Following Stratton<sup>21</sup> we can obtain power per unit volume from the scalar multiplication of  $\mathbf{E}$  and  $\mathbf{J}$ :

$$\mathbf{E} \cdot \mathbf{J} = \mathbf{E} \cdot (\nabla \times \mathbf{H}) - \mathbf{E} \cdot \frac{\partial \mathbf{D}}{\partial t} \quad (1.2.3)$$

using the identity

$$\nabla \cdot (\mathbf{E} \times \mathbf{H}) = \mathbf{H} \cdot (\nabla \times \mathbf{E}) - \mathbf{E} \cdot (\nabla \times \mathbf{H}) \quad (1.2.4)$$

and substituting in eq. (1.2.3), using eq. (1.2.2), we obtain

$$\mathbf{E} \cdot \mathbf{J} = - \left( \mathbf{E} \cdot \frac{\partial \mathbf{D}}{\partial t} + \mathbf{H} \cdot \frac{\partial \mathbf{B}}{\partial t} \right) - \nabla \cdot \mathbf{E} \times \mathbf{H} \quad (1.2.5)$$

Integrating over a volume  $V$  bound by a surface  $S$  we obtain

$$\int_V \mathbf{E} \cdot \mathbf{J} \, dV = - \int_V \left( \mathbf{E} \cdot \frac{\partial \mathbf{D}}{\partial t} + \mathbf{H} \cdot \frac{\partial \mathbf{B}}{\partial t} \right) dV - \int_S \mathbf{E} \times \mathbf{H} \, da \quad (1.2.6)$$

This result was first derived by Poynting in 1884. The vector

$$\mathbf{P} = \mathbf{E} \times \mathbf{H} \quad (1.2.7)$$

is defined as the Poynting vector.

The left hand side of eq. (1.2.6) represents the total power dissipated in the volume  $V$ . The first term of the right hand side represents stored energy inside volume  $V$ . The time average of the stored energy of sinusoidal fields is equal to zero. The second term on the right hand side of eq. (1.2.6) represents an electromagnetic energy flow across the surface bounding  $V$ .

The surface integral of the Poynting vector has thus a well defined meaning. The Poynting vector itself, has the dimension of power density, i.e., power per unit area.

### 1.3 The Electric Point Source

We will consider two types of point sources. The electric type, associated with an infinitesimal electric dipole, and the magnetic type, associated with an infinitesimal magnetic dipole. We will use complex notation as well as real time notation so as to be able to compare the two.

In spherical coordinates (see fig. 1.3.1), the field of an electric dipole in complex notation is\*

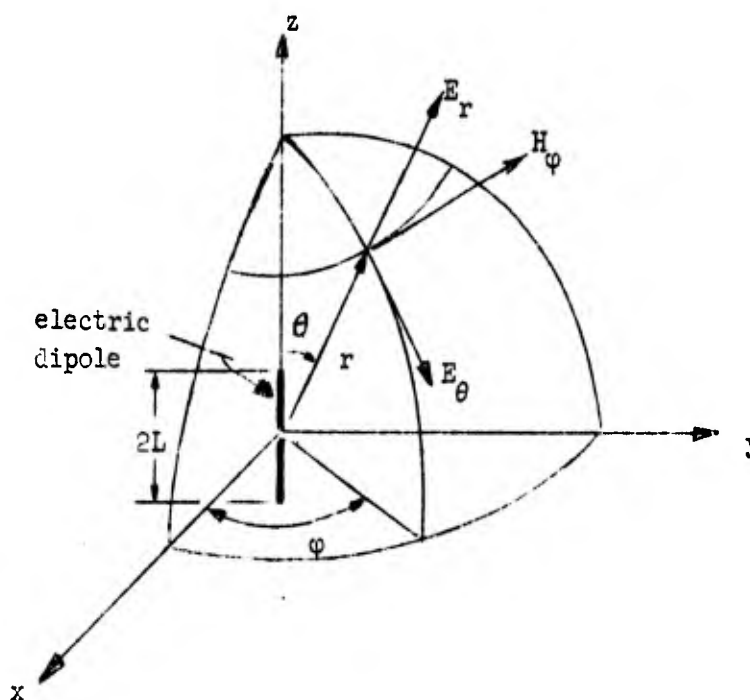


Figure 1.3.1 The Electric Dipole.

---

\* Ref. 20, p. 207; Ref. 17, p. 498.

$$E_r = \frac{|M|\beta^3}{4\pi\epsilon} e^{j\omega t'} \left[ \frac{2}{(\beta r)^2} + \frac{2}{j(\beta r)^3} \right] \cos \theta \quad (1.3.1)$$

$$E_\theta = \frac{|M|\beta^3}{4\pi\epsilon} e^{j\omega t'} \left[ -\frac{1}{j\beta r} + \frac{1}{(\beta r)^2} + \frac{1}{j(\beta r)^3} \right] \sin \theta \quad (1.3.2)$$

$$H_\varphi = \frac{\omega |M| \beta^2}{4\pi} e^{j\omega t'} \left[ -\frac{1}{j\beta r} + \frac{1}{(\beta r)^2} \right] \sin \theta \quad (1.3.3)$$

$|M|$  - electric moment

where

$$t' = t - \frac{\beta r}{\omega}$$

$$\beta = \omega \sqrt{\mu\epsilon} = \frac{2\pi}{\lambda}$$

$$|M| = |I_e(0)| \cdot \ell; \ell = \int_{-L}^L \left| \frac{I_e(z)}{I_e(0)} \right| dz$$

$|M|$  - magnitude of dipole moment

$\lambda$  - wavelength

$\epsilon$  - dielectric constant

$\omega$  - radian frequency

$r$  - distance from source.

In real-time notation\* we can rewrite the above equations as follows:

$$E_r = \frac{|M|\beta^3}{4\pi\epsilon} \cos \theta \left[ \frac{2 \cos \omega t'}{(\beta r)^2} + \frac{2 \sin \omega t'}{(\beta r)^3} \right] \quad (1.3.4)$$

$$E_\theta = \frac{|M|\beta^3}{4\pi\epsilon} \sin \theta \left[ -\frac{\sin \omega t'}{\beta r} + \frac{\cos \omega t'}{(\beta r)^2} + \frac{\sin \omega t'}{(\beta r)^3} \right] \quad (1.3.5)$$

$$H_\phi = \frac{\omega |M|\beta^2}{4\pi} \sin \theta \left[ -\frac{\sin \omega t'}{\beta r} + \frac{\cos \omega t'}{(\beta r)^2} \right] \quad (1.3.6)$$

### 1.3.1 Associated Impedances and Phase

Dimensionally, the ratio of E and H is an impedance. This concept of impedance holds in a retarded field and can be applied therefore to the above equations. We can define the following two impedances

$$Z_{\theta\phi} = \frac{E_\theta}{H_\phi} \quad (1.3.7)$$

and

$$Z_{r\phi} = \frac{E_r}{H_\phi} \quad (1.3.8)$$

From equations (1.3.1) to (1.3.3) we obtain accordingly

$$Z_{\theta\phi} = \sqrt{\frac{\mu}{\epsilon}} \left[ \frac{(\beta r)^2}{1+(\beta r)^2} + \frac{1}{j\beta r [1+(\beta r)^2]} \right] \quad (1.3.9)$$

---

\* Ref. 15, p. 305.

and

$$Z_{r\varphi} = 2 \sqrt{\frac{\mu}{\epsilon}} \frac{\cot \theta}{j\beta r} \quad (1.3.10)$$

It is observed that the impedance  $Z_{r\varphi}$  is purely imaginary and  $Z_{\theta\varphi}$  is complex in the near field and approaches the real value  $\sqrt{\mu/\epsilon}$  as  $r$  approaches infinity.

Equation (1.3.7) can also be put in the following form

$$Z_{\theta\varphi} = |Z_{\theta\varphi}| e^{j\gamma} \quad (1.3.11)$$

where

$$|Z_{\theta\varphi}| = \sqrt{\frac{\mu}{\epsilon}} \frac{\sqrt{1 + (\beta r)^6}}{\beta r [1 + (\beta r)^2]} \quad (1.3.12)$$

and

$$\gamma = - \arctan \frac{1}{(\beta r)^3} \quad (1.3.13)$$

Later sections of the report will deal with ways to actually measure the impedances associated with a point source.

A case of subsequent interest is obtained when a constant phase  $\gamma_0$  is introduced in the E component. If this is considered, eq. (1.3.13) has to be modified and attains the form

$$\gamma = \gamma_0 - \arctan \frac{1}{(\beta r)^3} \quad (1.3.14)$$



### 1.3.2 Associated Power Flow

There are two types of power flow and consequently two Poynting vectors associated with the electric point source. One is in the radial direction and given by

$$P_{\theta\varphi} = E_{\theta} H_{\varphi} \quad (1.3.15)$$

the other is directed towards the Z-axis (fig. 1.3.1) and given by

$$P_{r\varphi} = E_r H_{\varphi} \quad (1.3.16)$$

The instantaneous power can be obtained from equations (1.3.4) to (1.3.6)

$$P_{\theta\varphi_{inst.}} = \frac{\omega |M|_{\rho}^2 k^3}{(4\pi)^2 \epsilon r^2} \sin^2 \theta \left[ \sin^2 \omega t' - \frac{2 \sin \omega t' \cos \omega t'}{\beta r} + \frac{\cos^2 \omega t' - \sin^2 \omega t'}{(\beta r)^2} + \frac{\sin \omega t' \cos \omega t'}{(\beta r)^3} \right] \quad (1.3.17)$$

and

$$P_{r\varphi_{inst.}} = \frac{\omega |M|_{\rho}^2 k^2}{8\pi^2 \epsilon r^3} \sin \theta \cos \theta \left[ -\sin \omega t' + \frac{\cos^2 \omega t' - \sin^2 \omega t'}{\beta r} + \frac{\sin \omega t' \cos \omega t'}{(\beta r)^2} \right] \quad (1.3.18)$$

The average power density per cycle for an electric point source is accordingly:

$$P_{\theta\phi} = \frac{|M|^2 \omega^4 \mu \sqrt{\mu\epsilon}}{3 \cdot 2 \cdot \pi^2 r^2} \sin^2 \theta = P_e \quad (1.3.19)$$

and

$$P_{r\phi} = 0 \quad (1.3.20)$$

The average power per cycle can be obtained directly from equations (1.3.1) to (1.3.3), since

$$P_{\theta\phi} = \frac{1}{2} \operatorname{Re} \left[ E_{\theta} H_{\phi}^* \right] = \frac{1}{2} \operatorname{Re} \left[ E_{\theta}^* H_{\phi} \right] \quad (1.3.21)$$

Complex notation is simpler to use but it yields of course, only the average value per cycle and not the instantaneous value.

A corollary to the above is the case where a phase shift  $\gamma_0$  is introduced in  $E_r$ , eq. (1.3.1) or eq. (1.3.4), relative to the H component. As will be shown subsequently this is an entirely practical situation. The net result is that the average power per cycle, obtained similarly to equations (1.3.19) and (1.3.20) will now be given by

$$P_{\theta\phi} = P_e \left[ \cos \gamma_0 + \frac{\sin \gamma_0}{(\epsilon r)^3} \right] \quad (1.3.22)$$

and

$$P_{r\varphi} = P_e \frac{2 \cotan \theta}{\beta r} \sin \gamma_0 \left[ 1 + \frac{1}{(\beta r)^2} \right] \quad (1.3.23)$$

It is noted that for  $\gamma_0 = 0$  the previous results, equations (1.3.19) and (1.3.20) are obtained. The phase  $\gamma_0 = 90^\circ$  has here the physical significance that the power thus measured is the average reactive power associated with the electric point source. Using complex notation this average reactive power is given by the imaginary part of the complex Poynting vector. Proof from equations (1.3.1) to (1.3.3) we obtain

$$P_{\theta\varphi \text{ imag.}} = \frac{1}{2} \operatorname{Im} \left[ E_\theta H_\varphi^* \right] = \frac{P_e}{(\beta r)^3} \quad (1.3.24)$$

$$P_{r\varphi \text{ imag.}} = \frac{1}{2} \operatorname{Im} \left[ E_r H_\varphi^* \right] = P_e \frac{2 \cotan \theta}{\beta r} \left[ 1 + \frac{1}{(\beta r)^2} \right] \quad (1.3.25)$$

To summarize then we have the following concepts. The average real power density flow, i.e. the power per unit area is the power actually radiated by the source in the radial direction. It decreases as  $1/r^2$  which is a required condition for physical reasons since no power is assumed lost or created in the medium. This power is given by eq. (1.3.19).

An average reactive power is also associated with the point source. It is that power which flows back and forth across a closed sphere and

averages out to zero for each complete cycle. It comprises energy momentarily stored by the electromagnetic field. This average reactive power is given by equations (1.3.24) and (1.3.25), or, if  $\gamma_0 = 90^\circ$ , by equations (1.3.22) and (1.3.23). The average power as a function of an arbitrary phase  $\gamma_0$  is given in equations (1.3.22) and (1.3.23).

Once the physical interpretation of the complex Poynting vector is clarified, real time notation can be dropped in favor of complex notation. This will be done henceforth.

#### 1.4 The Magnetic Point Source

The field of a magnetic dipole is, in complex notation,\*

$$H_r = \frac{|M_m| \mu^3}{4\pi} e^{j\omega t} \cos \theta \left[ \frac{2j}{(r)^2} + \frac{2}{(r)^3} \right] \quad (1.4.1)$$

$$H_\theta = \frac{|M_m| \mu^3}{4\pi} e^{j\omega t} \sin \theta \left[ -\frac{1}{r} + \frac{j}{(r)^2} + \frac{1}{(r)^3} \right] \quad (1.4.2)$$

$$E_\phi = \frac{\omega \mu |M_m| \mu^2}{4\pi} e^{j\omega t} \sin \theta \left[ \frac{1}{r} + \frac{1}{j(r)^2} \right] \quad (1.4.3)$$

where

$$|M_m| = \text{magnetic moment}$$

---

\* Ref. 20, p. 233.

The spherical coordinate system used is shown in fig. 1.4.1.

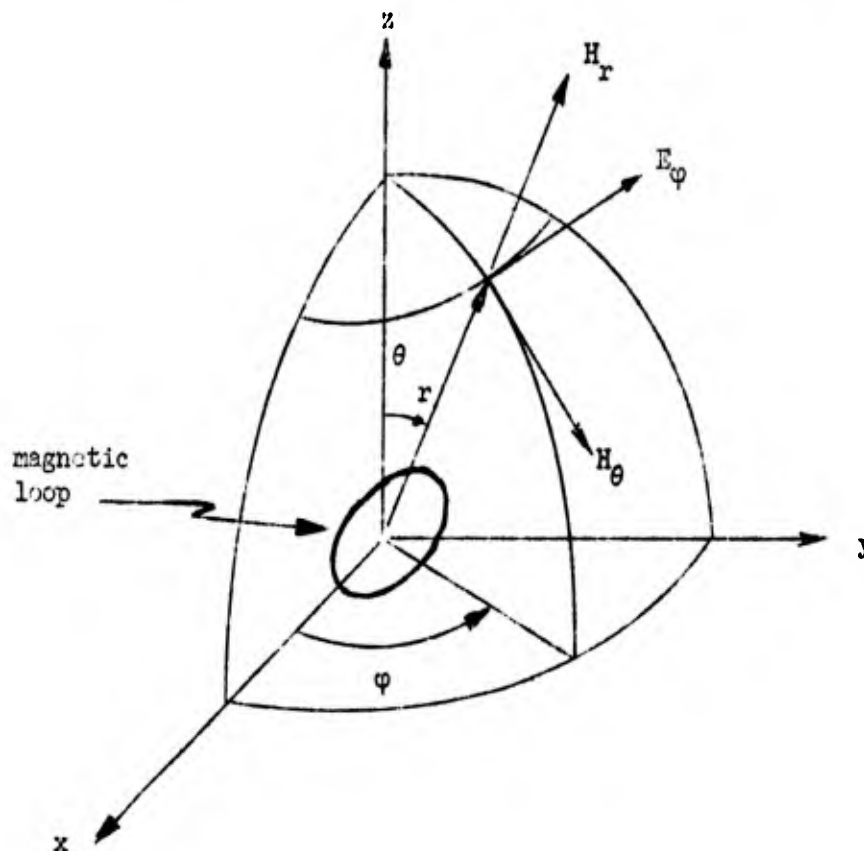


Figure 1.4.1 The Magnetic Dipole.

#### 1.4.1 Associated Impedances and Phase

Similar to sub-section 1.3.1 we can associate two impedances with the magnetic point source:

$$Z_{\phi\theta} = \frac{E}{H_{\theta}} = \sqrt{\frac{\mu}{\epsilon}} \left\{ \frac{-(\rho r)^4}{1 - (\rho r)^2 + (\rho r)^4} + \frac{\rho r}{j[1 - (\rho r)^2 + (\rho r)^4]} \right\} \quad (1.4.4)$$

and

$$Z_{\rho r} = \frac{E}{H_r} = \frac{3r}{2} \sqrt{\frac{\mu}{\epsilon}} \frac{\tan \theta}{j} \quad (1.4.5)$$

Equation (1.4.1) can be rewritten in the form

$$Z_{\varphi\theta} = |Z_{\varphi\theta}| e^{j\gamma} \quad (1.4.6)$$

where

$$|Z_{\varphi\theta}| = \sqrt{\frac{\mu}{\epsilon}} \frac{\beta r \sqrt{1 + (\beta r)^6}}{1 - (\beta r)^2 + (\beta r)^4} = \frac{\mu}{c} \beta r \sqrt{\frac{1 + (\beta r)^2}{1 - (\beta r)^2 + (\beta r)^4}} \quad (1.4.7)$$

and

$$\gamma = \arctan \frac{1}{(\beta r)^3} \quad (1.4.8)$$

Considering a phase  $\gamma_0$  in the E component we obtain, analogous to eq. (1.3.14),

$$\gamma = \gamma_0 + \arctan \frac{1}{(\beta r)^3} \quad (1.4.9)$$

#### 1.4.2 Associated Power Flow

Similar to eq. (1.3.21) we obtain the average radial power flow from the equation

$$P_{\varphi\theta} = -\frac{1}{2} \operatorname{Re} \left[ E_{\varphi} H_{\theta}^* \right] \quad (1.4.10)$$

The minus sign is required by definition of the outward flow. Compare fig. 1.4.1. Using eqs. (1.4.2) and (1.4.3) and introducing a phase shift  $\gamma_0$  in the E-component, we obtain

$$P_{\varphi\theta} = P_m \left[ \cos \gamma_0 - \frac{\sin \gamma_0}{(\nu r)^3} \right] \quad (1.4.11)$$

where

$$P_m = \frac{\omega \mu |M_m|^2 \nu^3}{2 (4\pi)^2 r^2} \sin^2 \theta \quad (1.4.12)$$

Again, similar to eq. (1.3.19),  $P_m$  stands for the average outward flow of power associated with a magnetic point source. Equation (1.4.11) is analogous to eq. (1.3.22) and the same comments apply. Confer subsection 1.3.2.

## 2. THEORETICAL CONSIDERATIONS

### 2.1 Introduction

This section deals with the theoretical aspects, from an elementary point of view, of the interaction effects that arise when dipole and loop antennas are used as sensors of the electromagnetic field in the vicinity of a transmitting antenna.

In particular section 2.2 is a summary of previous theoretical results\* and sections 2.3 and 2.4 a discussion of these results as applied to the case where the transmitting antenna comprises a short dipole.

---

\* Ref. 1, p. 18-26.

## 2.2 Interaction Errors of the Poynting Sensor

Figure 2.2.1 illustrates an essentially two dimensional situation. A magnetic sensor<sup>\*</sup>, i.e., a small loop, is centered on the geometric center of an electric sensor<sup>\*</sup>, i.e., a short dipole. This combination of sensors is referred to as a Poynting sensor<sup>\*\*</sup>. The Poynting sensor is removed a distance  $r$  from a transmitting antenna.  $I_t(\omega) e^{j\omega t}$  represents the input current to the transmitting antenna

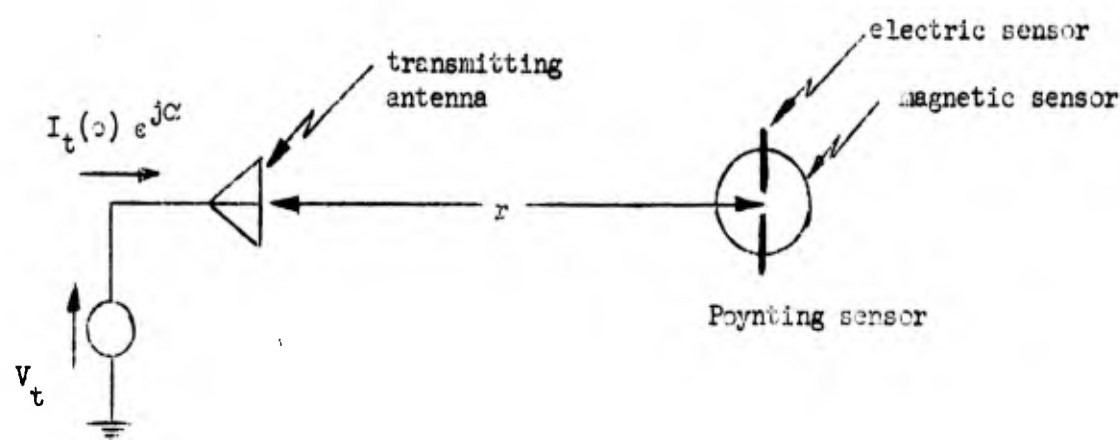


Figure 2.2.1 Poynting Sensor and Transmitting Antenna.

and  $V_t$  the source voltage. In the case of interest here the transmitting antenna comprises a short dipole parallel to the electric sensor.

The following nomenclature is adopted:

$Z_{tt}$  = self impedance of the transmitting antenna

$Z_{mm}$  = self impedance of the magnetic sensor

\* Ref. 1, p. 10-14.

\*\* Ref. 1, p. 18.



$Z_{ee}$  = self impedance of the electric sensor

$Z_{tm}$  = mutual impedance between the transmitting antenna and the magnetic sensor

$Z_{te}$  = mutual impedance between the transmitting antenna and the electric sensor

$Z_{em}$  = mutual impedance between the electric and magnetic sensors

$R_{ml}$  = load resistance of magnetic sensor

$R_{el}$  = load resistance of electric sensor

$V_m$  = load voltage of magnetic sensor

$V_e$  = load voltage of electric sensor

$K_m = Z_{mm}/R_{ml}$

$K_e = Z_{ee}/R_{el}$

$H$  = the measured\* magnetic field at the Poynting sensor perpendicular to the plane of the magnetic sensor

$E$  = the measured electric field at the Poynting sensor parallel to the electric sensor

$H_t$  = the true\* magnetic field at the Poynting sensor perpendicular to the plane of the magnetic sensor

$E_t$  = the true electric field at the Poynting sensor parallel to the electric sensor

$l$  = effective length of the transmitting dipole (a function\*\* of the dipole length  $2L$ )

$a = \mu\omega\pi\left(\frac{D}{2}\right)^2$  where  $\frac{D}{2}$  is the radius of the magnetic sensor

---

\* Ref. 1, pp. 8-10, 23.

\*\* Ref. 1, p. 12.

Assuming  $Z_{em} = 0$ , it has been shown\* that

$$\begin{aligned} \frac{E}{E_t} = \frac{H}{H_t} &= \frac{Z_{tt} R_{e\ell} R_{m\ell} (1 + K_e) (1 + K_m)}{Z_{tt} R_{e\ell} R_{m\ell} (1 + K_e)(1 + K_m) - Z_{te}^2 R_{m\ell} (1 + K_m) - Z_{tm}^2 R_{e\ell} (1 + K_e)} \\ &= \frac{1}{1 - Z_{te}^2 / Z_{tt} R_{e\ell} (1 + K_e) - Z_{tm}^2 / Z_{tt} R_{m\ell} (1 + K_m)} \end{aligned} \quad (2.2.1)$$

In addition, it has been shown\*\* that

$$V_e = \frac{-E\ell}{1 + K_e} \quad V_m = \frac{jHa}{1 + K_m} \quad (2.2.2)$$

and

$$Z_{tm} = \frac{jH_t a Z_{tt}}{V_t} \quad (2.2.3)$$

Letting  $R_{e\ell} = \infty$  the situation depicted in fig. 2.2.1 reduces to that of interaction solely between the transmitting antenna and the magnetic sensor. Accordingly, (2.2.1) becomes

$$\frac{H}{H_t} = \frac{1}{1 - Z_{tm}^2 / Z_{tt} R_{m\ell} (1 + K_m)} \quad (2.2.4)$$

In like manner,  $E/E_t$  for the case of interaction solely between the transmitting antenna and the electric sensor becomes

---

\* Ref. 1, pp. 19 and 24.

\*\* Ref. 1, pp. 22-23.

$$\frac{E}{E_t} = \frac{1}{1 - Z_{te}^2 / \sqrt{\mu_0 \epsilon_0} R_{e2} (1 + K_e)} \quad (2.2.5)$$

Interaction phase and magnitude errors are defined\* by the relations

$$\left| \frac{E}{E_t} \right| - 1 = \text{interaction magnitude error of the electric sensor}$$

$$\text{ph} \frac{E}{E_t} = \text{interaction phase error of the electric sensor}$$

$$\left| \frac{H}{H_t} \right| - 1 = \text{interaction magnitude error of the magnetic sensor}$$

$$\text{ph} \frac{H}{H_t} = \text{interaction phase error of the magnetic sensor}$$

Thus, by (2.2.1), the interaction errors of the electric and magnetic sensors forming the Poynting sensor are identical. As a result (2.2.2) shows that

$$\text{ph} V_e - \text{ph} V_m = \text{ph} E_t - \text{ph} H_t + \gamma_0 \quad (2.2.6)$$

where

$$\gamma_0 = \text{ph} \left[ - \frac{1+K_m}{(1+K_e)j} \right] \quad (2.2.7)$$

In other words, the phase difference between the load voltages of the electric and magnetic sensors is identical to that between the true electric and magnetic fields  $E_t$  and  $H_t$  except for the additive constant  $\gamma_0$ .

---

\* Ref. 1, p. 24.

In addition, it is self evident from (2.2.1), (2.2.4), and (2.2.5) that for a given transmitting antenna the interaction errors of the electric and magnetic sensors will decrease as the self impedances of these devices increase. Conversely, for a given electric and/or magnetic sensor the interaction errors should decrease with an increase in the self impedance of the transmitting antenna.

### 2.3 Interaction Errors in the Presence of a Short Dipole Transmitting Antenna.

In the case where the transmitting antenna of fig. 2.2.1 comprises a short dipole E and H are given by\*

$$E = j \sqrt{\frac{\mu}{\epsilon}} \frac{|I_t(0)| l}{2\lambda r} \left(1 + \frac{1}{j\beta r} - \frac{1}{\beta^2 r^2}\right) e^{j(\alpha - \beta r)} \quad (2.3.1)$$

$$H = j \frac{|I_t(0)| l}{2\lambda r} \left(1 + \frac{1}{j\beta r}\right) e^{j(\alpha - \beta r)} \quad (2.3.2)$$

by eq. (2.2.2)

$$\frac{V_e}{V_m} = - \frac{(1+K_m) l}{(1+K_e) ja} \frac{1}{\beta r} \frac{\beta r + j(\beta^2 r^2 - 1)}{1 + j\beta r} \quad (2.3.3)$$

therefore,

$$\begin{aligned} \text{ph } V_e - \text{ph } V_m &= \arctan \frac{\beta^2 r^2 - 1}{\beta r} - \arctan \beta r + \gamma_0 = \\ &= \arctan \frac{1}{\beta^3 r^3} + \gamma_0 \end{aligned} \quad (2.3.4)$$

---

\* Ref. 1, pp. 12-13.

where  $\gamma_0$  is given by eq. (2.2.7) and is completely determined by the self impedances and load resistances of the electric and magnetic sensors comprising the Poynting sensor.

Consider the case where  $R_{el} = \infty$ , i.e., interaction solely between the transmitting dipole and the magnetic sensor. By eq. (2.2.3) and eq. (2.3.2)

$$Z_{tm} = \frac{j \pi^3 \mu \left(\frac{D}{2}\right)^2 \omega^3 l}{2 c^2 \beta^2 r^2} (1 + j\beta r) e^{-j\beta r} \quad (2.3.5)$$

As a rough approximation of the self inductance  $L_m$  of the magnetic sensor take\*

$$L_m = \left(\frac{D}{2}\right) \mu \left[ \ln \left(\frac{8D}{2r_0}\right) - 2 \right] \quad (2.3.6)$$

where  $r_0$  represents the radius of the wire forming the magnetic sensor.

The self reactance of the transmitting dipole can be approximated by resorting to data of the type provided in reference 15, p. 364. Dimensions of a magnetic sensor and transmitting dipole approximating the devices used in experiments reported later in this report are  $2L = .16$  m, dipole thickness = .001 m,  $D = .06$  m,  $r_0 = .0005$  m, and  $R_{ml} = 50 \Omega$ . At 400 mc, neglecting the radiation resistances of the magnetic sensor and transmitting dipole, these values, via eq. (2.2.4), yield an interaction magnitude error less than 7% for  $r = 1.5$  cm and essentially 0% for  $r > 6$  cm.

---

\* Ref. 17, p. 260.

#### 2.4 Remarks on the Impedance Concept

The impedance concept described in section 2.2 as a model of interaction between antennas separated by distances less than a wavelength is rather crude. However, its simplicity and apparent ability to describe, at least in a semi-quantitative sense, the situations considered in this report seem to justify its use. A more rigorous and accurate analysis would, for example, involve the overpowering task of solving the boundary value problem for each case considered.

The model of interaction used is subject to several restrictive assumptions. For example, the largest dimensions of the magnetic and electric sensors should be much less than both wavelength and the distance between the sensor and transmitting antenna.\* In the example cited in the latter part of section 2.3 there is a violation of the second assumption. Yet, the results obtained are consistent with the experimental data shown in Section 3. Moreover, (2.3.4) is verified to within very small distances of separation between the transmitting antenna and the Poynting sensor.

The self reactance of a short dipole increases drastically with increasing wavelength.\*\* Therefore, referring to (2.2.1), the interaction errors of the Poynting sensor in the case of a short dipole transmitting antenna should decrease with decreasing frequency. However, for a fixed wavelength the self reactance of a short dipole decreases with increasing dipole length. As a result, the interaction errors of the Poynting sensor should decrease at a fixed frequency with decreasing dipole length. Again

---

\* Ref. 1, pp. 10, 12, 14.

\*\* Ref. 15, p. 364.

these observations are confirmed by the results obtained in Section 3. In addition, it is readily apparent from (2.2.1) that the interaction errors of the Poynting sensor can be controlled by the load resistances of the electric and magnetic sensors.

### 3. NEAR FIELD MEASUREMENTS OF ELECTRIC AND MAGNETIC FIELD COMPONENTS

#### 3.1 Introduction

Various concepts and properties of the near field of point sources were described in Section 1 of this report. The problem of testing those properties by actual measurements is discussed in this and the following section. The first requirement for such measurements is the development of appropriate field sensors. This problem was discussed and analyzed in previous reports and additional problems in Section 2 of the present report. As a result, it was decided to use as sensors small dipoles and loops, sensitive and accurate enough for near field use, yet unhampered to a large extent by interaction. The use of an image plane was found to be advantageous in demonstrating the principle of the measurements. The present section discusses the equipment and sensors used in those measurements.

#### 3.2 Practical Near-Field Sensors

From considerations reported in Section 2 of this report as well as from earlier reports it was decided that dipoles short compared to wavelength and loops whose diameter is small compared to wavelength are usable as near-field probes of electromagnetic radiation.

This decision was based on the following specific points.

1. The small electric and magnetic sensors can be used as true indicators of the electric and magnetic field components respectively. In reference 1, p. 14, it was shown that the load voltage of a small electric dipole is proportional to the total magnitude of E existing in the direction of the dipole. Similarly, the load voltage of a magnetic dipole was shown to be directly proportional to the magnitude of the total H existing in the perpendicular direction of the loop. Barring interaction, the sensors were considered as true field indicators. This assertion has been verified independently in other laboratories since the appearance of the above report.<sup>7</sup>

2. Interaction error is reduced compared to the half wave dipole. The interaction magnitude error and phase error between two sensors can essentially be neglected when separated by a distance comparable to their own dimensions. Interaction errors have been discussed extensively in reference 1.

There appeared a number of difficulties using small sensors as field indicators. One of the difficulties is the sacrifice in sensitivity of the probe when its dimensions are reduced. Lack of sensitivity is not a primary cause for concern, since expected signals in the near field are relatively large. As a secondary symptom, however, due to the relatively more significant pickup through lead cables the effectiveness of the sensors was reduced. As shown in Appendix B the effect of finite gaps in short dipoles can no longer be ignored.

Experiments were conducted to establish the practical limits within which small sensors can be used effectively. Experiments were performed in the 100-400 Mc range. Small dipoles ranging in length from 2 to 20 cm



were used. Shielded loops ranging in diameters from 1 to 15 cm were also used. A balun was usually employed in connection with the dipoles. The different experimental setups included dipole-dipole, dipole-loop and loop-loop measurements in free space. In all experiments of this type it was found that leads were a major source of error and, in fact, interacted severely with other objects in the field. The effectiveness of the small sensors thus impaired, a different approach was required.

One suggested approach was the introduction of an image plane, described in the following subsection.

### 3.3 The Image Plane and its Sensors

A successful simulation of free space that eliminated the effects of antenna leads was provided by an image plane.

The image plane consisted initially of a copper mesh 6 feet by 6 feet. It was later found necessary to double its size. The initial experiment included measurements between two monopoles, one of which was fixed at one point in the plane, the other movable with respect to the first. One problem automatically eliminated by the use of monopoles rather than dipoles was the balun. The monopole consisted in each case simply as a piece of wire extending the center conductor of the coaxial lead cable through the screen. One monopole served as a transmitting source, the other as a receiver. The amplitude of the received signal as a function of distance from the transmitting source is shown in fig. 3.3.1. The amplitude of the transmitter is held constant. Measurements were performed at three frequencies, 20 Mc, 200 Mc, and 400 Mc. Two different dipole lengths were used: 2 cm and 8 cm. Excellent agreement with the theoretical curve was obtained in all cases. The measurements at a distance of 1 cm varied, however, considerably due to the interaction of the sensors.

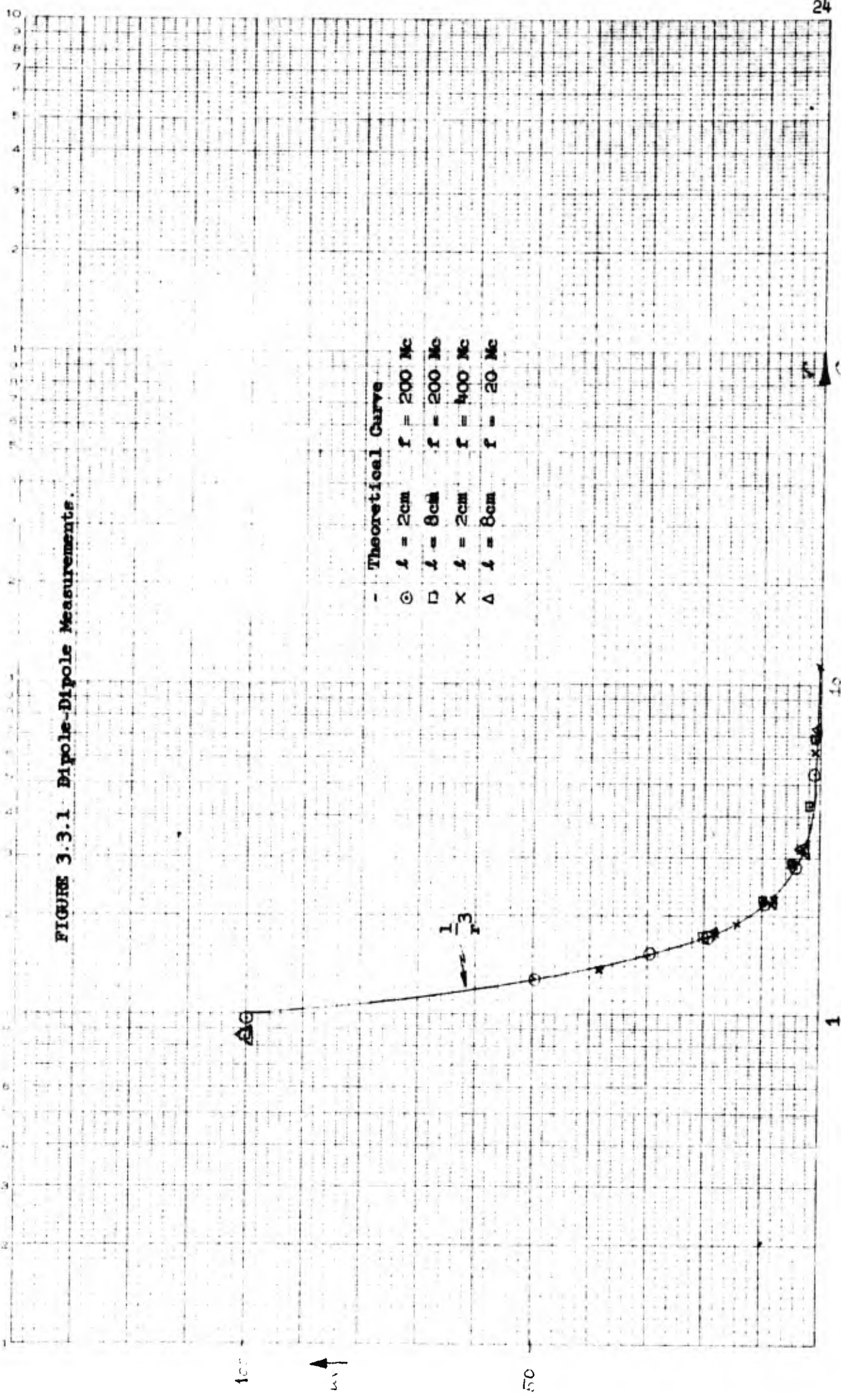


FIGURE 3.3.1 Dipole-Dipole Measurements.

The magnetic analog of the monopole over an image plane is the semicircular loop. The principle of operation can be explained from fig. 3.3.2.

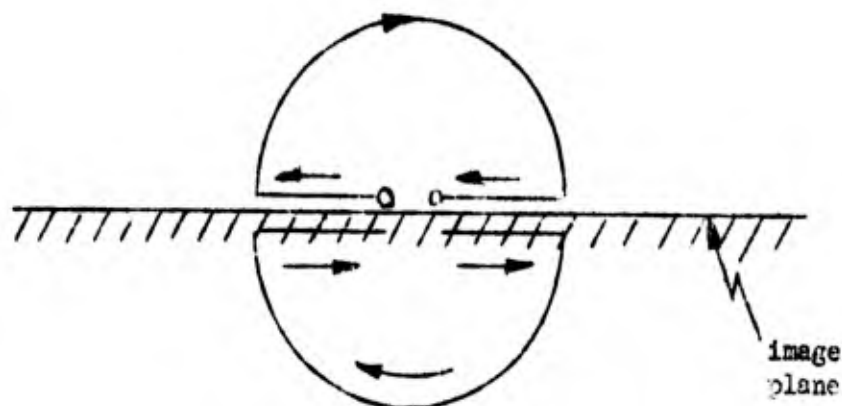


Figure 3.3.2 Principle of Operation of Semicircular Loop.

As seen from fig. 3.3.2 the currents along the horizontal feeding line are in opposite direction above and below the image plane and therefore cancel with respect to an external object. The current in both semiloops are in the same direction and therefore the semiloop over an image plane will have the same electromagnetic field as a loop in free space. The practical advantage is the fact that lead wires, just as in the case of the monopole, are conveniently below the image plane and therefore do not interfere with the operation of the loop.

In practice, a shielded semiloop was used to cancel effects of the electric field as in the case of a shielded loop in free space.

The directional properties of the semiloop were obtained by measuring its radiation pattern. They were found to be identical to those of a loop in free space. Results of this measurement are shown in fig. 3.3.3.

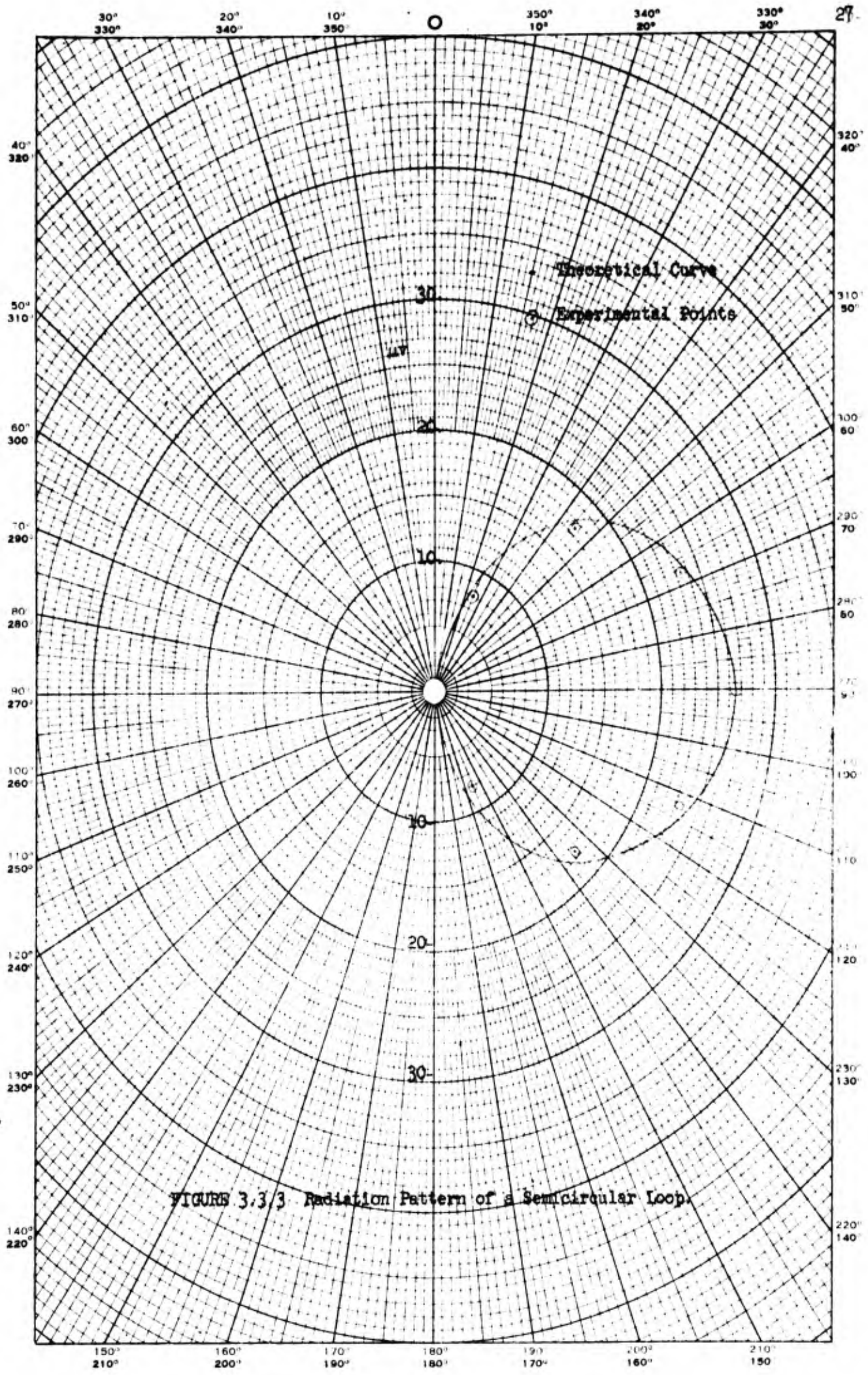
Measurements were taken, using a shielded semiloop and a monopole and another experiment using two semiloops. In each case the amplitude vs. distance was measured, one sensor serving as transmitter, the other as a receiver of that signal. Results of these measurements are shown in figs. 3.3.4 and 3.3.5.

As a result of the previous measurements it was established that the near-field sensors as described above conformed to expected behavior as field sensors and their mutual interaction was of negligible proportions. The basis for the development of more sophisticated sensors, as described in Section 4 of this report, was thus obtained.

#### 3.4 The Instrument Setup

The instrumentation required for amplitude measurements was relatively simple. One receiver of the type AN/URM-47 covering the frequency range of 20-400 Mc was used. The signal generator was a Hewlett-Packard, Model 608A, covering the frequency range 10-500 Mc.

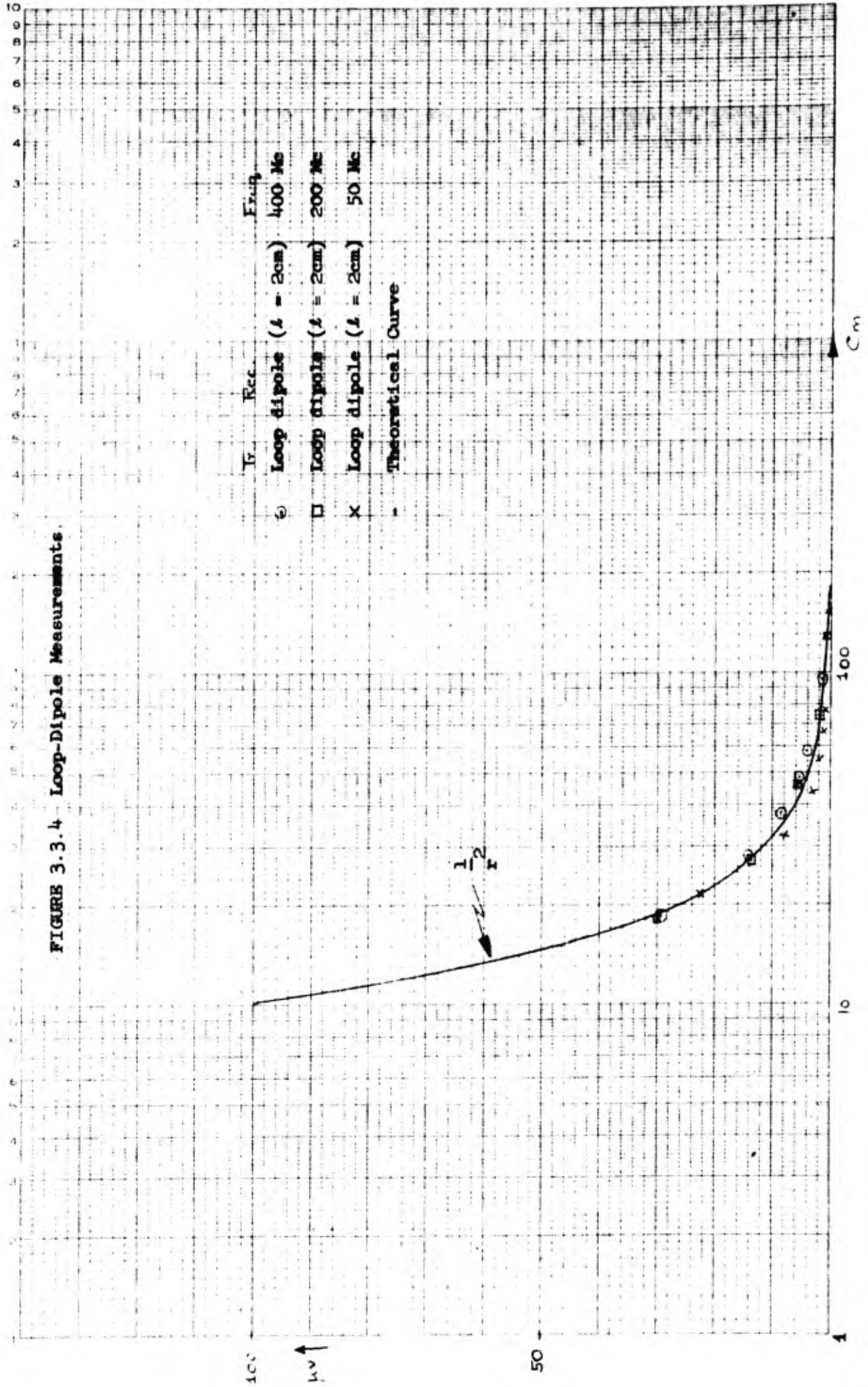
No arrangements were provided to obtain an impedance match between instrument and sensors. Such an impedance match over the frequency range of interest would have presented difficulties outweighing its possible benefits.



EUGENE DIETZGEN CO.  
PRINTED IN U.S.A.

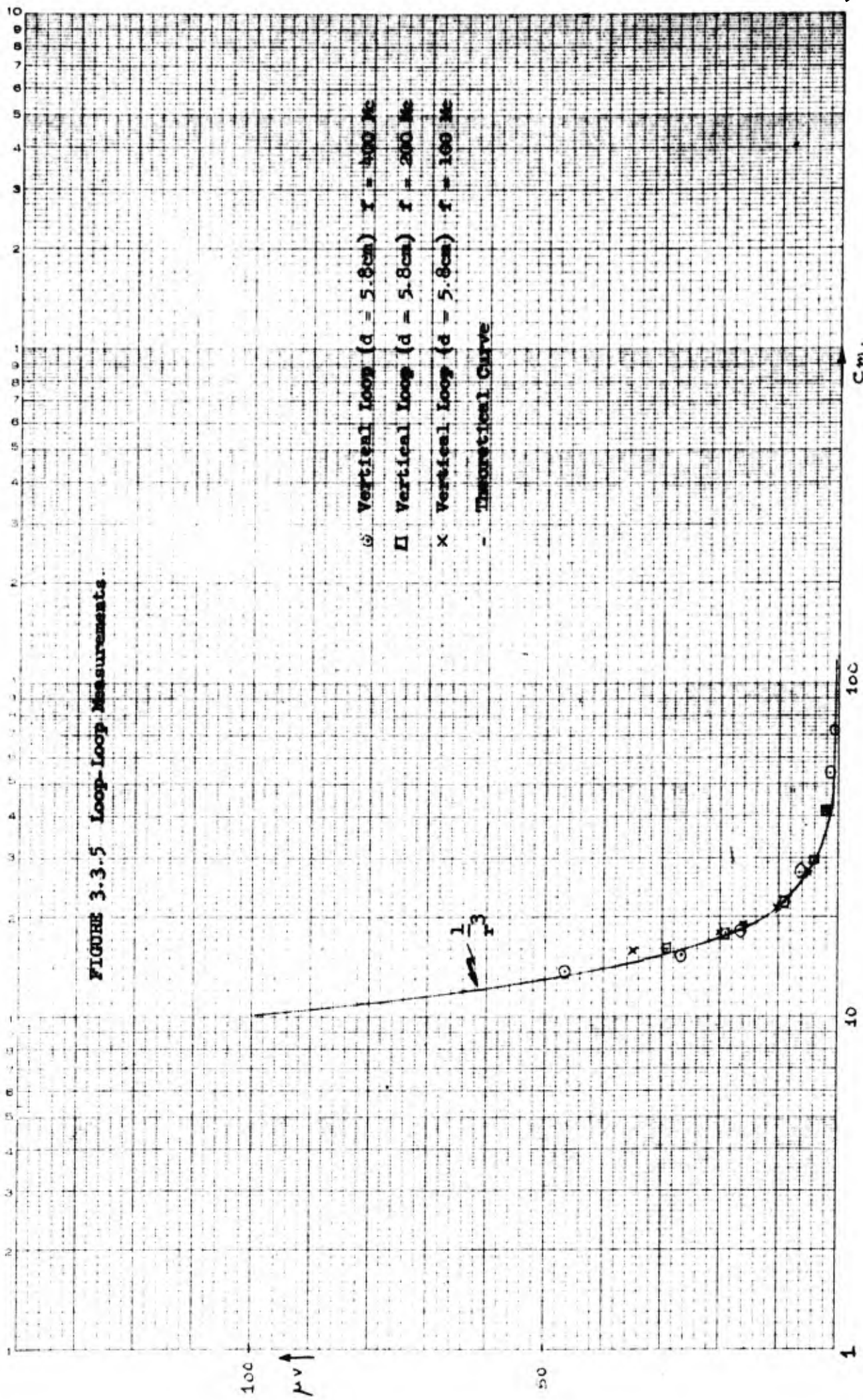
NO. 340-11 DIETZGEN GRAPH PAPER  
POLAR CO-ORDINATE

FIGURE 3.3.3 Radiation Pattern of a Semicircular Loop.



NO. 4000-110-0101ZIGEN PAPER  
SEMI-LOG GRAPH  
4 5/8" x 10" 100 100 PER 100

FIGURE 3.3.5 Loop-Loop Measurements.



100  
μV ↑

1

10

100

C.m.

#### 4. POWER AND PHASE MEASUREMENTS IN THE NEAR FIELD

##### 4.1 Introduction

The measurement of individual electric and magnetic field components using small sensors in the near field, as described in the previous section, confirmed the anticipated behavior of both sensors and point sources. Using this as a basis, simultaneous measurements of electric and magnetic field components were attempted. Specially modified sensors and instruments were used for this purpose. Additional information about near field measurements was thus obtained and compared to the theoretical results of Section 1.

The present section describes the experimental setup and the resulting measurements of the near field properties of point sources.

##### 4.2 The Poynting Sensor

A sensor capable of measuring E and H independently, instantaneously and simultaneously at a point in space will be called a Poynting sensor.

From theoretical considerations discussed in Section 1 the short dipole and small loop antennas met the requirements of measuring instantaneously E and H respectively at a point in space. The next step required to combine the two sensors so that they would not interfere with each other and thus providing the possibility of making simultaneous measurements of E and H at a point in space.

As a starting point in the development of the Poynting sensor loop-dipole measurements of the kind described in the previous section were carried out. The measurements were carried out both in free space and above an image plane. As expected, the signal received by the electric



sensor (dipole or monopole) when it was moved parallel to the loop, attained a maximum near the loop wire and a minimum when closest to the loop center. Measurements taken when both sensors were nearly overlapping were critical with respect to position.

The object of the above measurements was to establish in practice a configuration in which the effect of one sensor on the other is minimized.

The most satisfactory results were obtained in the case where the monopole was located directly in the center of the semicircular loop. The attenuation of the signal received by the monopole in this position was about 40 db below the maximum. This combination of monopole and loop seemed therefore to satisfy the initial requirements of a Poynting sensor.

To further test the apparent property of negligible interaction between the semicircular loop and the monopole an additional movable monopole was used. Previous loop-dipole and dipole-dipole experiments were then repeated, using the movable monopole as the transmitting source and either the semicircular loop or the monopole part of the Poynting sensor as a receiver. In both cases the identical results to those described in figs. 3.3.1 and 3.3.4 were obtained.

From the above described measurements a Poynting sensor, consisting of a semicircular shielded loop and a center monopole, seemed to satisfy, within practical limits, the design goals set for such a sensor. A picture of the Poynting sensor is shown in fig. 4.4.1.

The next and final step required a simultaneous measurement of E and H and the phase between the two as a function of distance from the radiating source. Phase measurements required instrumentation beyond that

described in subsection 3.4. The necessary experimental setup is accordingly described next.

#### 4.3 The Instrument Setup

For simultaneous measurements of E and H two receivers of the type AN/URM-47 were used. The input of one was connected to the semicircular loop and the other to the monopole located at its center. The condition for simultaneous and independent measurements of E and H at a point in space were thus essentially provided for.

To measure phase between the two received signals the above receivers had to be modified. Since they are heterodyne receivers, their internal oscillators had to be synchronized. In practice, the internal oscillators were disconnected and an external oscillator used for both receivers. The external oscillator was tuned to a frequency of 15 Mc above the received signal. The 15 Mc IF outputs of the two receivers were then fed to a sensitive voltmeter capable of reading each output individually as well as their instantaneous difference. A block diagram of the experimental setup is shown in fig. 4.3.1.

The most accurate measurement of phase at 15 Mc was found to be the triangular method necessitating three measurements: the RMS outputs of the two receivers  $V_1$  and  $V_2$  and the instantaneous difference  $V_1 - V_2$  between the two. The phase  $\gamma$  could accordingly be obtained graphically from the plot of the triangle as shown in fig. 4.3.2 or of course from the formula

$$\gamma = \cos^{-1} \frac{V_1^2 + V_2^2 - (V_1 - V_2)^2}{2V_1V_2} \quad (4.3.1)$$

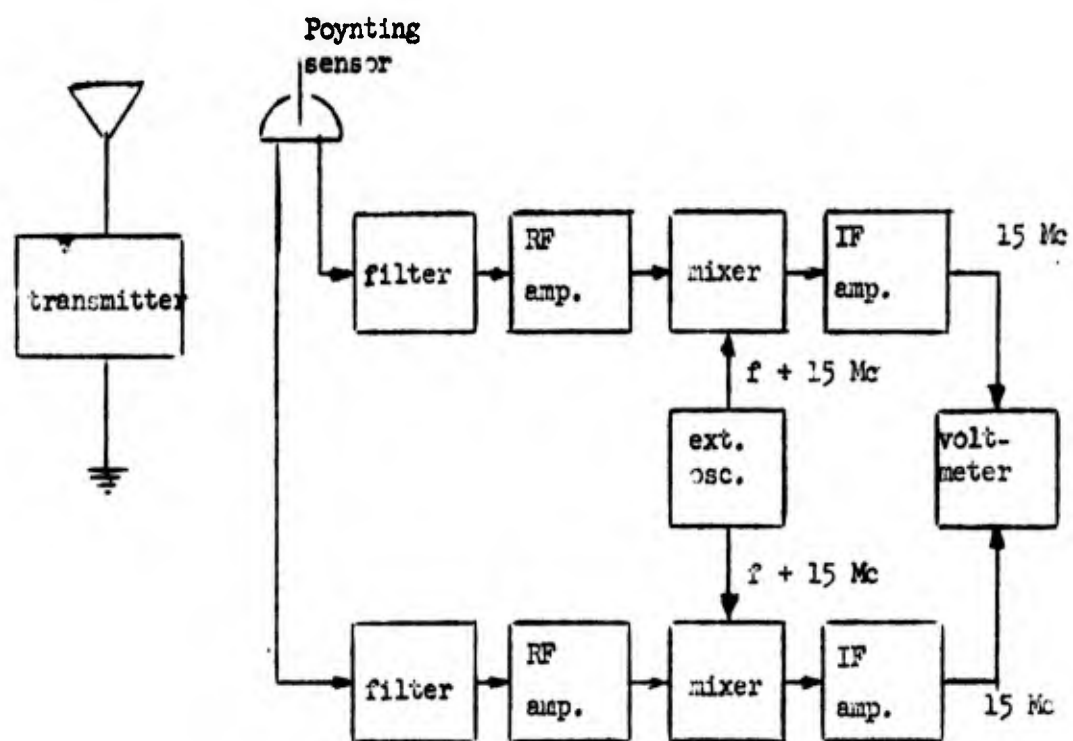


Figure 4.3.1 Block Diagram for Phase Measurements.

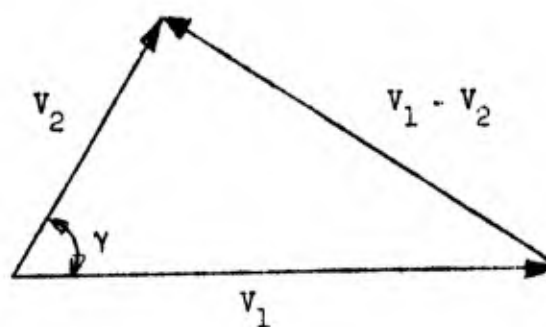


Figure 4.3.2 Vector Diagram for Phase Measurements.

#### 4.4 Phase Measurements

The equipment described in the previous subsection was capable of measuring phase of an electromagnetic field with a resolution of about  $1^\circ$ . The noise level made the measurement of phase at low signal levels much less accurate. Phase measurements with the given setup provided no way of differentiating between positive and negative phases.

The first set of measurements included the Poynting sensor as the receiving element and an electric point source as the transmitter. The corresponding arrangement, including the image plane, is pictured in fig. 4.4.1.

For practical convenience the transmitting monopole was the movable element. The monopole was moved in intervals, from a distance of about 7 cm from the center of the Poynting sensor to a distance of about 1 m from the sensor. Measurements were taken at 230 Mc. At this frequency the border of the near field, defined as  $\lambda/2\pi$ , was equal to a distance of 20.7 cm from the radiating source. This distance was right within the range of measurements. Keeping the transmitter power constant, the output signals of the Poynting sensor were measured at each interval. The magnitude of the E and H components of the electromagnetic field were already discussed in Section 3 and the results plotted in figs. 3.3.1 and 3.3.5.

The phase between E and H at each point in space can be predicted for the electric source from equation (1.3.14), repeated here for convenience.

$$\gamma = \gamma_0 - \arctan \left( \frac{\lambda}{2\pi r} \right)^3 \quad (1.3.14)$$

The value of  $\gamma_0$  is affected by numerous factors, the most important of which are:

1. A constant phase angle may be introduced by the two receivers. Tuning one or both of the receivers will affect this phase considerably because of the dependence of phase response of a receiver on tuning.

In Section 1, theoretical account has been taken of this phase by the introduction of a phase shift between the E and H components.  $\gamma_0$  in that case was the corresponding relative phase shift.

2. In Section 2, eq. (2.2.7), the dependence of  $\gamma_0$  on the load impedances of the magnetic and electric sensor comprising the Poynting sensor was discussed. It is therefore evident that the receiving sensors do not have to be conjugately matched to serve as Poynting sensors. A mismatch, or any match, will only affect the value of the constant phase  $\gamma_0$ .
3. If the Poynting sensor is so oriented in space as to measure  $E_r$ , part of the phase angle will be due to  $Z_{rp}$ , eq. (1.3.10)<sup>r</sup>. This phase angle will depend on orientation and will be constant as long as the orientation of the Poynting sensor is not changed.

There may be other factors affecting the value of  $\gamma_0$  such as the skin effect as discussed in Appendix A, or the effect of a finite gap as discussed in Appendix B, or possible unbalance of the feeding line.  $\gamma_0$  is in effect a summation of all constant phases (with respect to distance from source) due to any of the above reasons. The actual value of  $\gamma_0$  is obtained from experiments. It is the asymptotic value of phase at a large distance from the source.

In all of the above cases, care must be taken that throughout the taking of measurements,  $\gamma_0$  is not changed. Once an instrument setting is obtained, it is only permitted to change distance between transmitting source and Poynting source. Almost any other adjustment, such as receiver tuning, will affect phase via  $\gamma_0$ . This introduces a practical difficulty since the dynamic range close to the radiating source changes drastically with distance. Any adjustment of an attenuator runs the risk of affecting the phase behavior of the instrument. Care had to be exercised to prevent this from happening.

From all of the above it is seen that the phase as a function of distance, eq. (1.3.14), is unaffected as long as reasonable care is taken during the measurements. The resulting phase function will be indicative of the source.

In fig. 4.4.3 the phase measurements are given for an electric source. The magnitudes of E and H as a function of distance are plotted in fig. 4.4.4. All three of those measurements correspond closely to the theoretical curves of Section 1 and thus verify the assumptions made.

The value of  $\gamma_0$  could be varied simply by detuning one of the receivers slightly. Measurements were accordingly taken at different values of  $\gamma_0$ .

Figure 4.4.5 was taken with  $\gamma_0$  adjusted to  $48^\circ$ . Since no provisions existed in the given instrument setup to differentiate between positive and negative phase angles, i.e., E leading or lagging with respect to H, all phase angles were plotted as positive numbers. Equation (1.3.14) has to be modified accordingly since only magnitudes were obtained:

FIGURE 4.4.3 Phase Measurements of Electric Source

$$d = 1.5 \text{ cm}$$

$$\chi = \delta_0 - \arctan\left(\frac{\lambda}{2\pi d}\right)^3$$

$$\delta_0 = 90^\circ$$

$\delta$   
 $90^\circ$

$45^\circ$

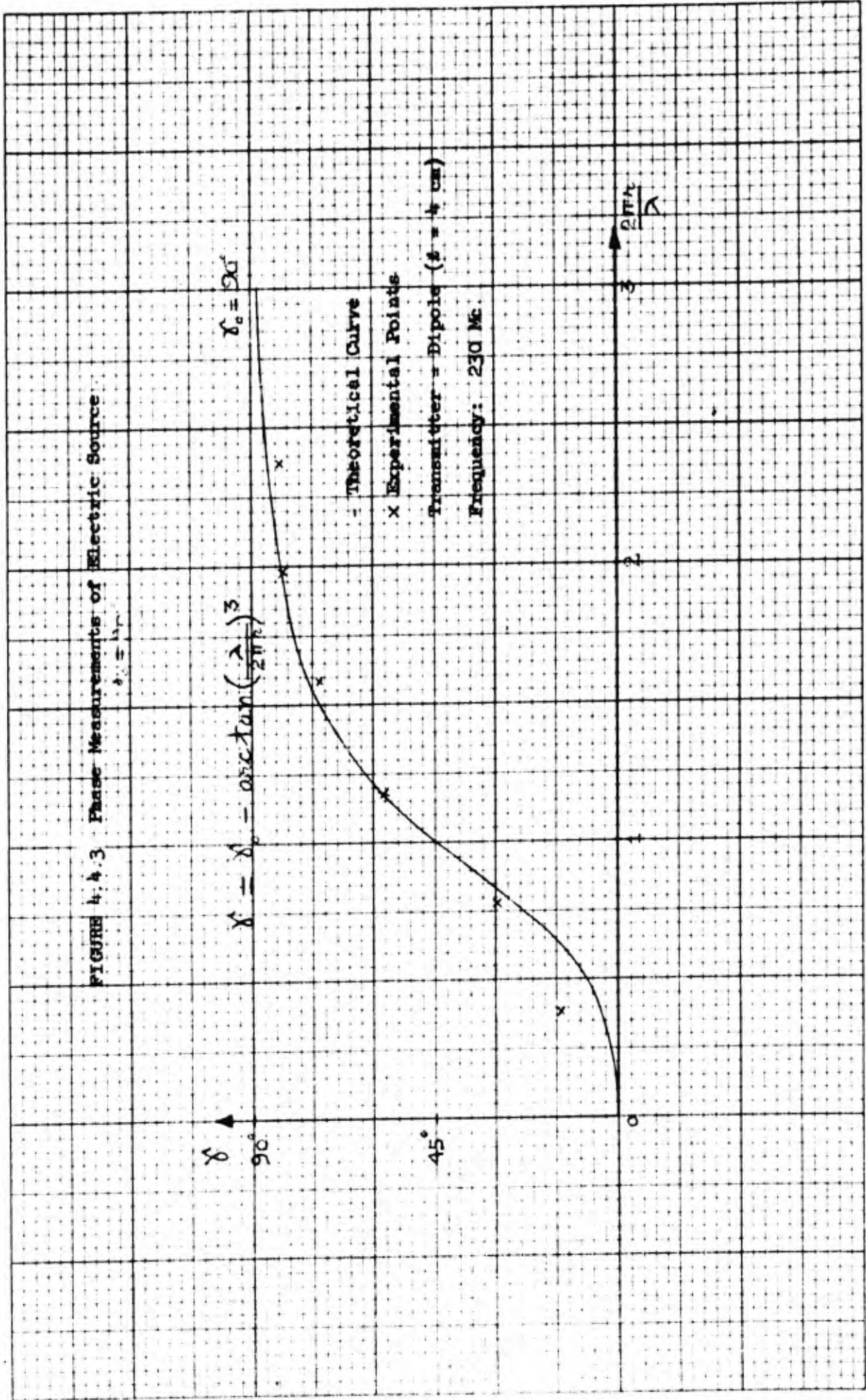
- Theoretical Curve

X Experimental Points

Transmitter = Dipole ( $l = 4 \text{ cm}$ )

Frequency: 230 Mc.

$\frac{2\pi r}{\lambda}$



NO. 310 5010 DIEZIGEN 3485 PAPER  
 SEMI LOG. 100 CM. C.  
 4 CYCLES X 100 DIV. 1000 PER INCH

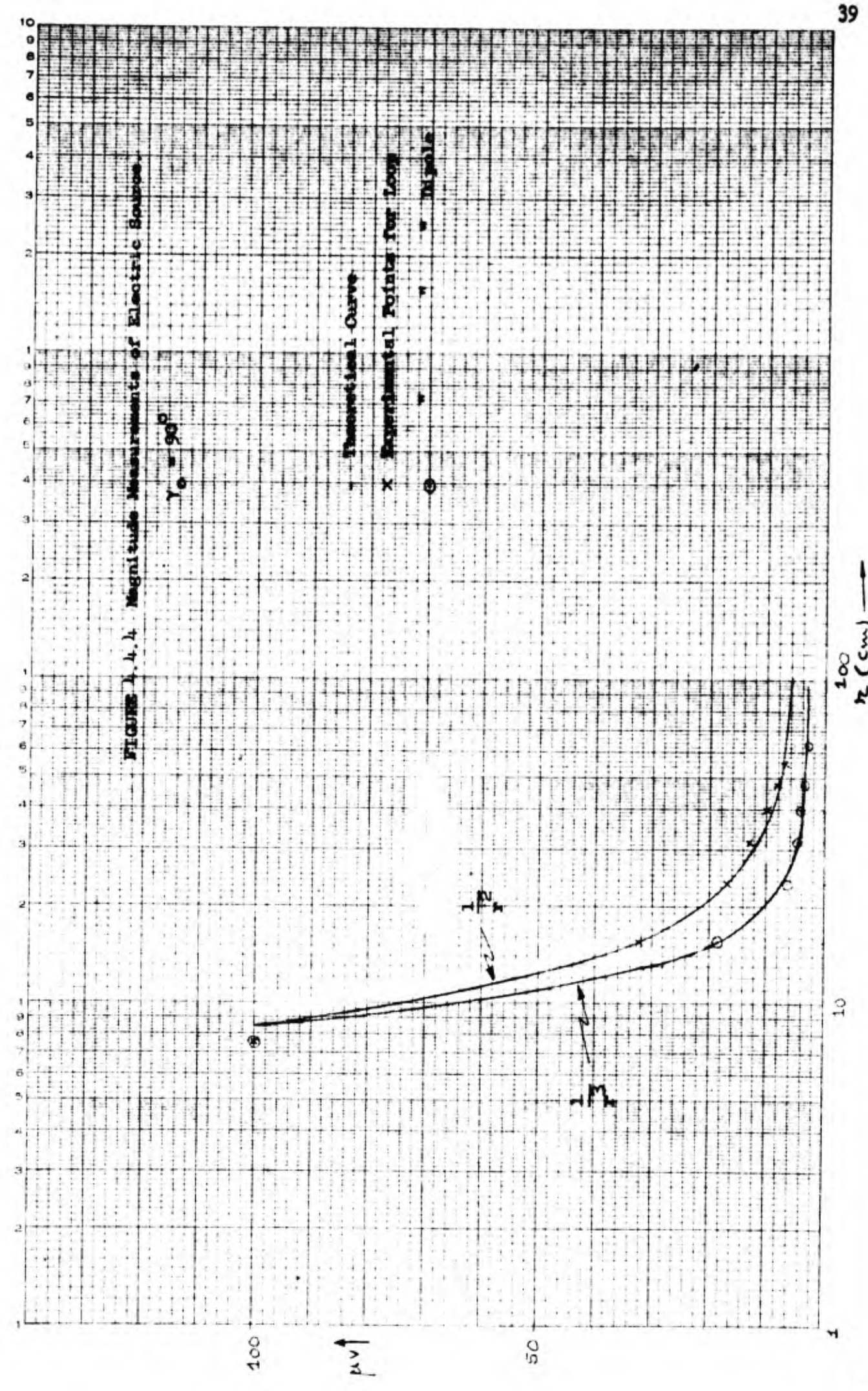


FIGURE 1.4.4 Magnitude Measurements of Electric Bores.



$$\gamma = \left| \gamma_0 - \arctan \left( \frac{\lambda}{2\pi r} \right)^3 \right| \quad (4.4.1)$$

The corresponding theoretical curves and the measured points are given in figs. 4.4.5 and 4.4.7. The variation of the magnitudes of E and H as a function of distance are unaffected by the value of  $\gamma_0$  as seen from a comparison of figs. 4.4.4 and 4.4.6, where each corresponds to a different value of  $\gamma_0$ .

To complete the set of measurements a magnetic source consisting of a semicircular loop was substituted for the electric source and measurements repeated. A picture of the corresponding setup is shown in fig. 4.4.2.

As seen from eq. (1.4.9) the only expected difference from previous results is a difference in sign. The resultant theoretical curves and measured points are shown in figs. 4.4.8 and 4.4.9.

The average power per unit area, i.e.,  $EH \cos \theta$ , delivered by the dipole in fig. 4.4.1 is shown in fig. 4.4.10. The experimental values for E, H and  $\theta$  are taken from figs. 4.4.4 and 4.4.3 with  $\theta = \gamma_0 - \gamma$ . Very good agreement is obtained except for the point of closest measurement at 7.5 cm. The discrepancy here results primarily from the measured value of  $\theta$  which also appears in fig. 4.4.3. Measured values of  $\theta$  consistently seems to be in error at the closest distances. The reason for this is not completely understood at the present time, but it is believed to occur because of interaction. The distances are, however, closer than would be involved in any practical measurement procedure.

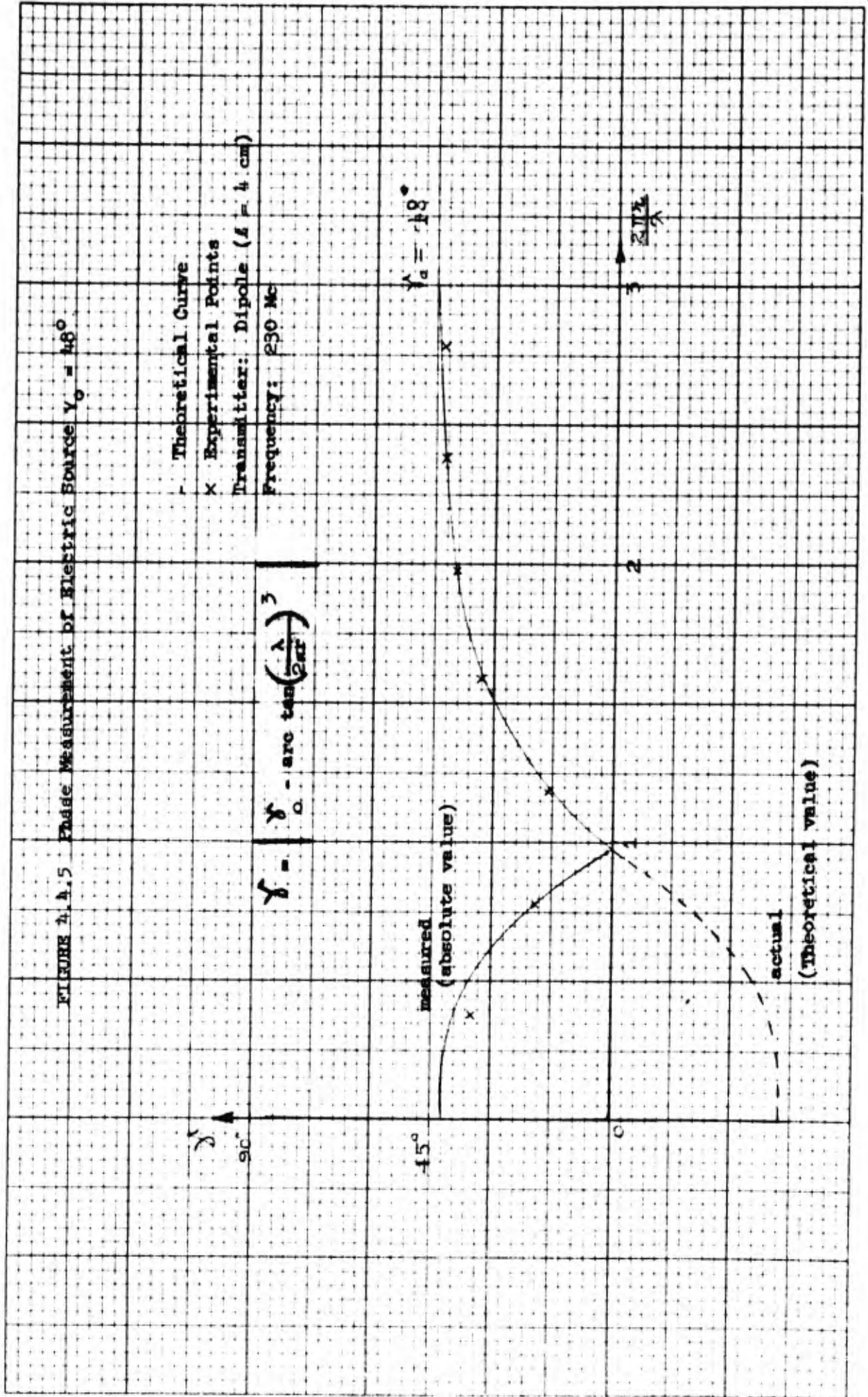
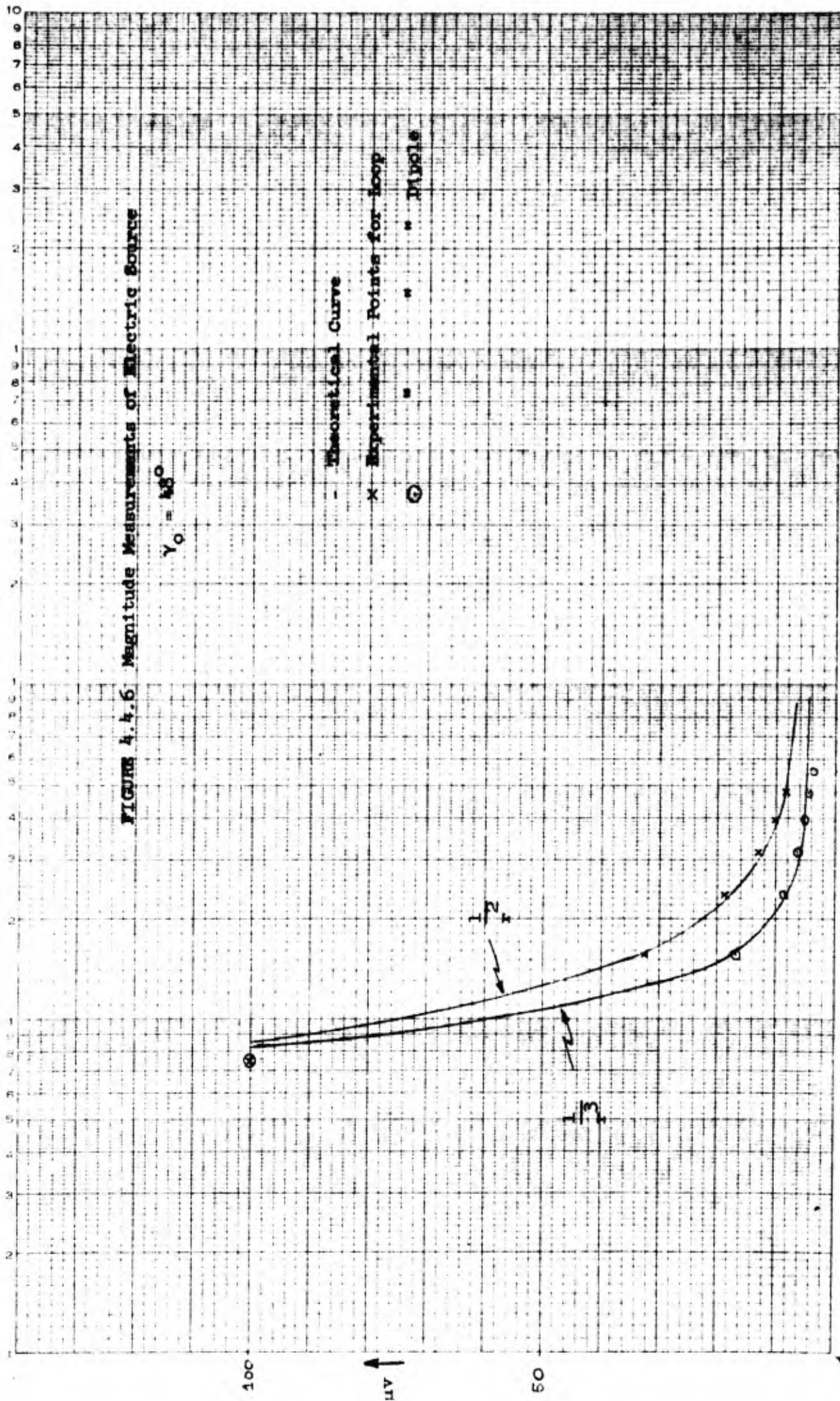
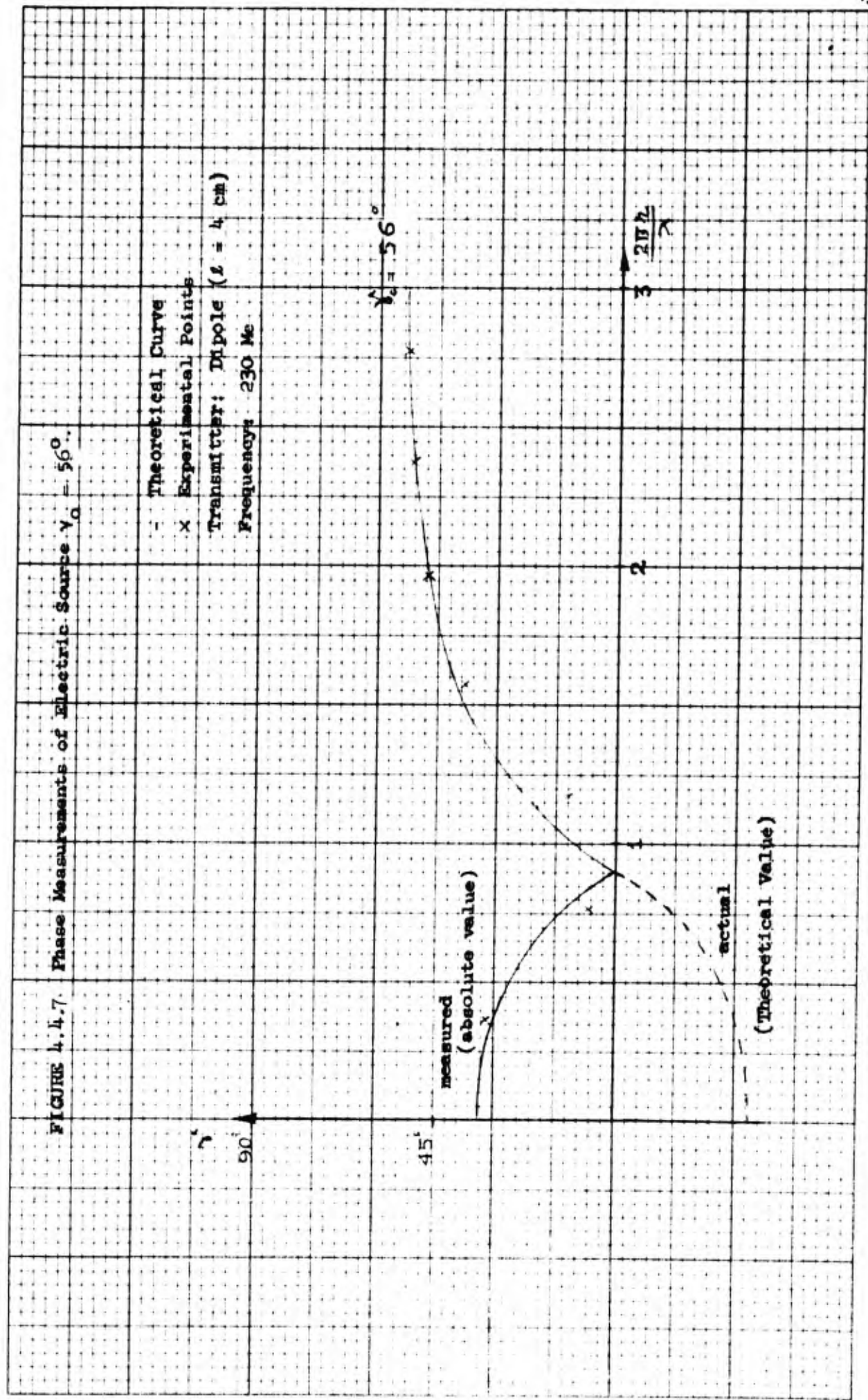


FIGURE 4.4.6 Magnitude Measurements of Electric Source

$\gamma_0 = 45^\circ$



U.S. GOVERNMENT PRINTING OFFICE: 1964 O 354-114



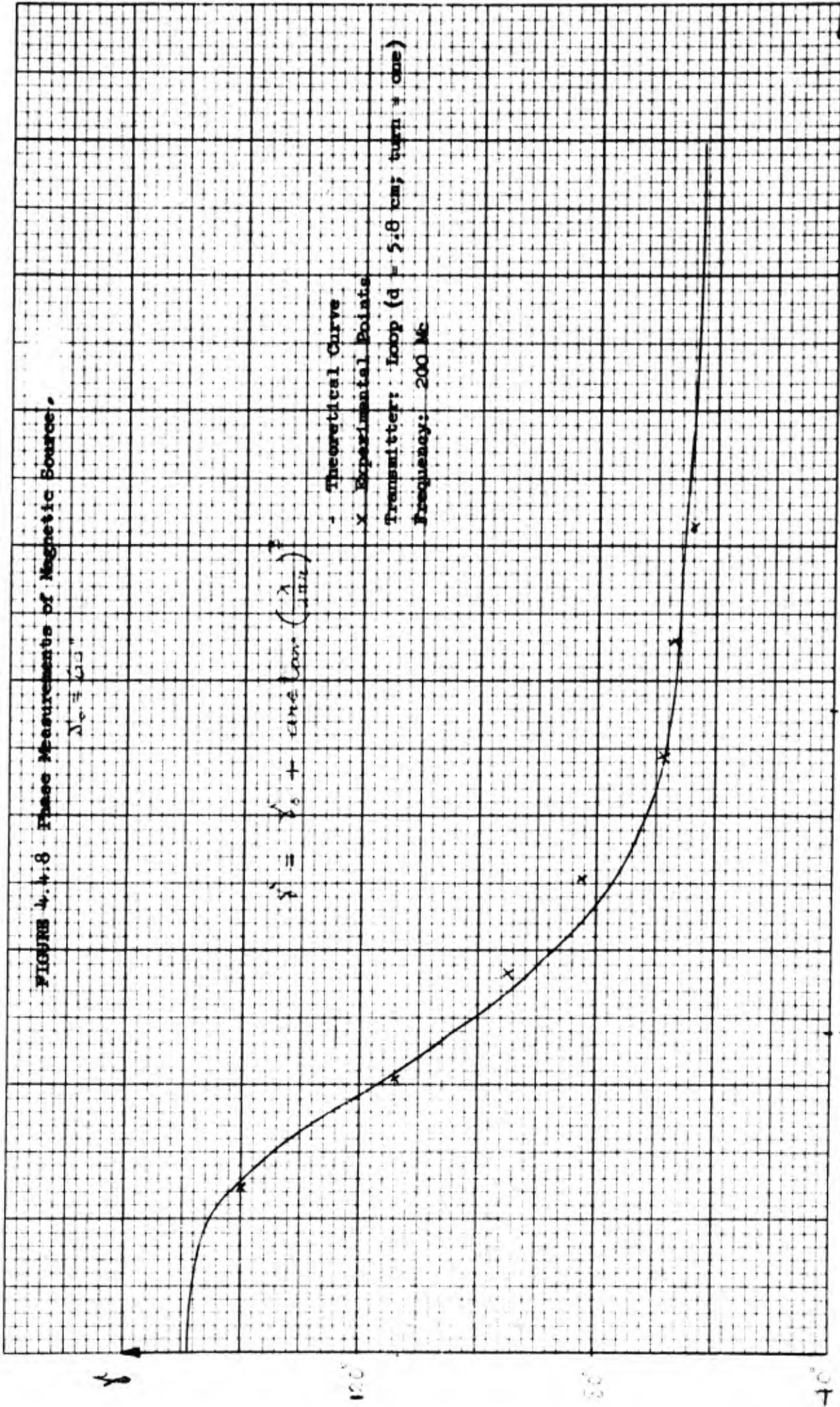
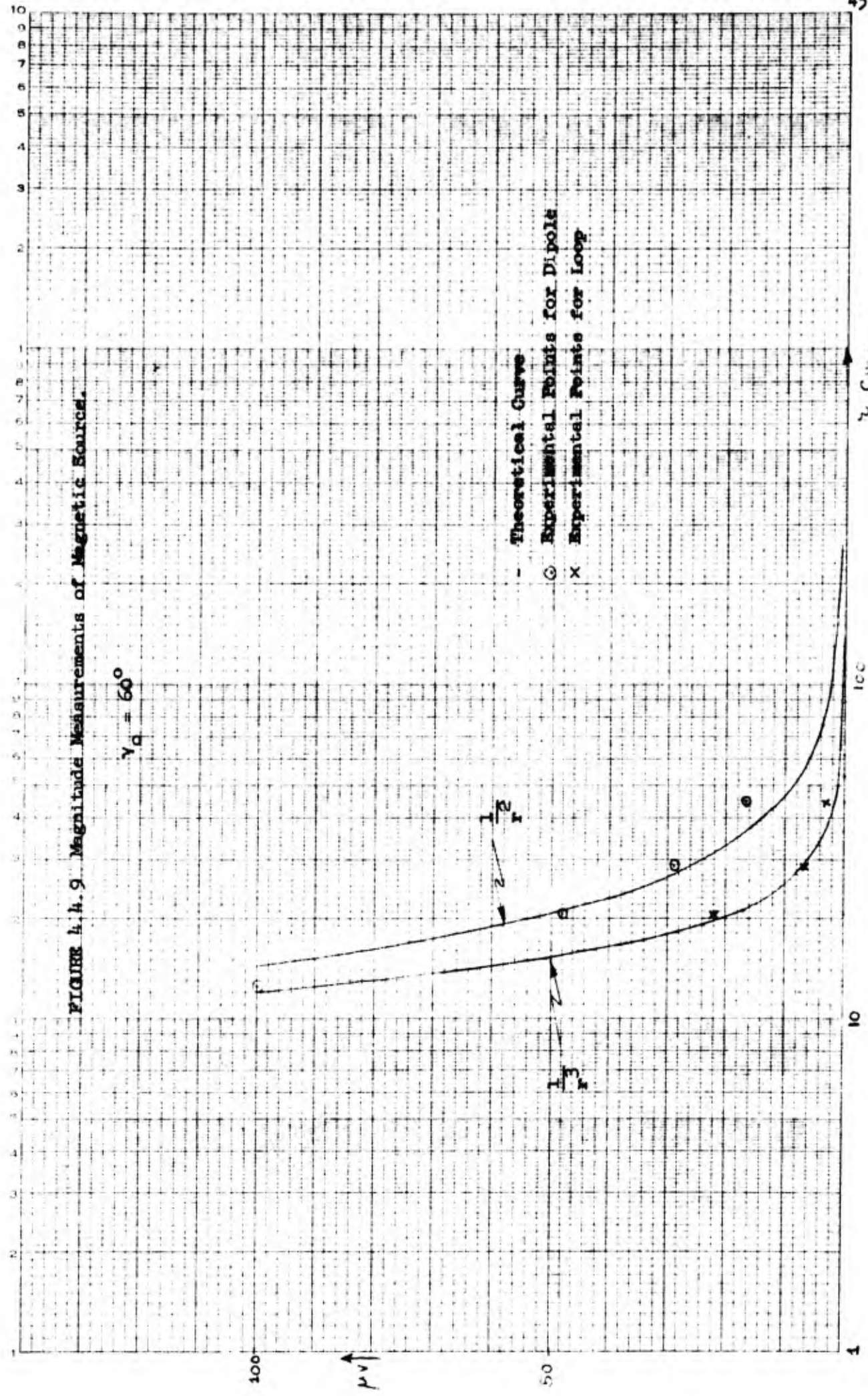
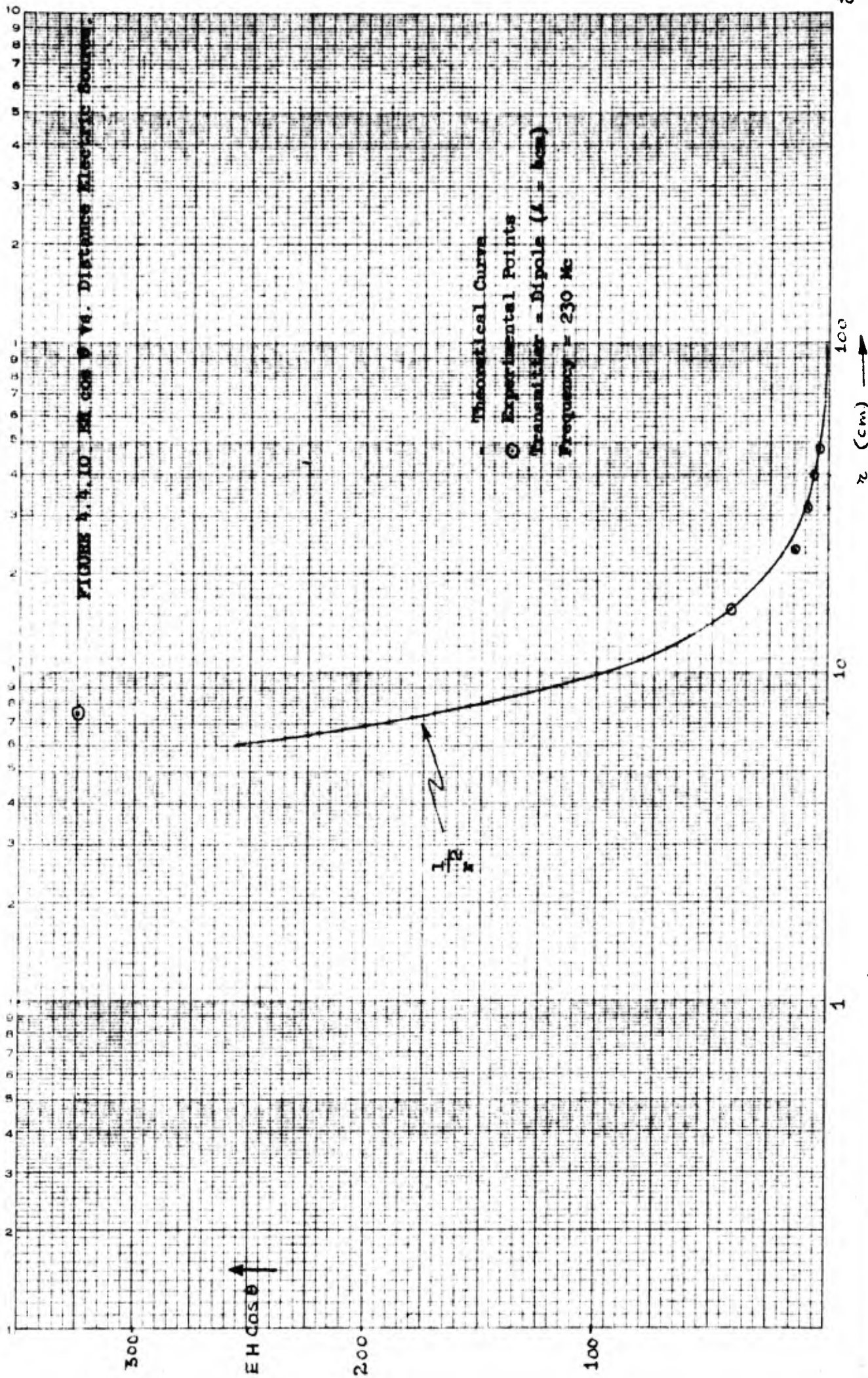


FIGURE 4.4.9 Magnitude Measurements of Magnetic Source.



U.S. GOVERNMENT PRINTING OFFICE: 1964 O 353-730

NO. 340 LINDQVIST'S CHART PAPER  
 5 CM. LOGAR. THIN  
 4 CYCLES X 0.5 DIVISIONS PER INCH



#### 4.5 Summary and Conclusions

The measured data agreed closely with theoretical curves. The fundamental properties of electric and magnetic sources are therefore subject to practical measurements. As shown in this report actual near field measurements of electric and magnetic sources is feasible and can provide the information regarding power flow in the far field.

The phase measurements had the advantage of a relatively unperturbed pattern in the near field. Most experimental and practical errors affected the phase only through a constant which, if care is exercised, does not affect the general shape of the phase curve. The only effect of different values of this constant is a parallel shift of the entire curve. In particular it is noted that the phase error of a Poynting sensor due to interaction is cancelled as shown in eq. (2.2.6). The measurement of phase seems therefore a more accurate measurement in the near field than the measurement of either E or H.

Depending on instrumentation designed specifically for the purpose, the actual values of the real or the imaginary Poynting vectors can be obtained directly.

In this report, only a demonstration of the principle involved in Poynting and phase measurements was attempted. For this reason the image plane served a very useful purpose. For practical situations it will be necessary to develop a Poynting sensor which performs satisfactorily in free space.

Additional studies and experimental evidence are necessary to determine the applicability of Poynting vector and phase measurements to other than point sources and when exposed to other than simple sine waves.



Appendix AINTERNAL RESISTANCE OF CYLINDRICAL DIPOLE ANTENNAA.1 Introduction

Most of antenna theory assumes that the antenna is perfectly conducting. In practice, however, the material of which a dipole antenna is made has finite conductivity such that internal impedance arises from this conductivity. Based on a simplified model, error in input impedance due to the finite conductivity is estimated in this section.

A.2 Calculation of Internal Impedance

If the conductivity of dipole material is finite, the current density at high frequencies is concentrated near the surface due to "skin effect". Therefore it is immaterial to distinguish whether the dipole is a solid or tubular cylindrical conductor as far as internal impedance is concerned.

To calculate internal impedance it is assumed that current is in the axial direction only, and that current variation in the axial or circumferential direction is negligible compared to that in the radial direction. Then the internal impedance per unit length of circular cylinder, whose radius is  $a$ , is given by<sup>17,21</sup>

$$z_d = \frac{\sqrt{j\omega\mu\sigma}}{2\pi\sigma a} \frac{J_0(\sqrt{j\omega\mu\sigma} a)}{J_1(\sqrt{j\omega\mu\sigma} a)} \quad (\text{A.1})$$

where

$$\omega = 2 \pi f$$

$f$  = frequency in cps

$\mu$  = permeability of dipole material

$\sigma$  = conductivity of dipole material

$J_0, J_1$  = Bessel functions of first kind of zero and first order respectively

For very high frequencies it can be approximated as

$$z_d = \frac{1}{2a} \sqrt{\frac{f\mu}{\pi\sigma}} (1 + j) \quad (\text{A.2})$$

A good approximation is  $\mu = \mu_0$  and  $\epsilon = \epsilon_0$  for most dipole antenna materials. The conductivity of standard copper (I.A.C.S.)<sup>14</sup> is  $5.8 \times 10^7$  mhos/m, of commercial grade copper is  $5 - 10 \times 10^7$  mhos/m and of commercial grade brass is  $1 - 5 \times 10^7$  mhos/m.

Total internal impedance of cylindrical dipole antenna whose length is  $2L$  is approximately given by

$$\begin{aligned} Z_d &= R_d + j X_d = 2z_d L \\ &= \frac{L}{a} \sqrt{f} \sqrt{\frac{\mu}{\pi\sigma}} (1 + j) \text{ ohms} \end{aligned} \quad (\text{A.3})$$

where

$R_d$  = internal resistance

$X_d$  = internal reactance

For more exact total internal impedance effective dipole length instead of actual length should be used, but for simplicity the above form, which introduces a negligible amount of difference, is used. If the dipole is made of standard copper  $\mu = \mu_0 = 4\pi \times 10^{-7}$  henries/m and  $\sigma = 5.8 \times 10^7$  mhos/m and accordingly

$$Z_d = 8.3 \frac{L}{a} \sqrt{f} (1 + j) \times 10^{-8} \text{ ohms} \quad (\text{A.4})$$

### A.3 Comparison of Internal and Radiation Resistances

The calculated value of internal resistance is compared with the radiation resistance of center driven cylindrical dipole antenna which is obtained by Schelkunoff and Friis.<sup>19</sup> As shown in fig. A.1 even at 10 Gc the internal resistance  $R_d$  of a dipole is negligible compared to the radiation resistance  $R_a$  if  $a/\lambda$  is larger than  $\frac{1}{100}$  where  $\lambda$  is wavelength. It is noticed that, however, if the dipole is very thin, the internal resistance is comparable with radiation resistance when  $L/\lambda$  is less than  $\frac{1}{10}$ . In particular, at 10 Gc it is shown that the internal resistance is greater than radiation resistance. Noting that, when dissipation in feeding line are neglected, the input resistance of a dipole is given by<sup>14</sup>

$$R_i = \left| \frac{I_o}{I_i} \right|^2 (R_a + R_d)$$

where

$R_i$  = input resistance

$I_i$  = input current

$I_o$  = current amplitude on dipole

internal resistance should be included for the calculation of input resistance when the dipole is very short and thin.

As shown in figs. A.2 and A.3, the influence of internal resistance on input resistance is negligible when  $L/\lambda$  varies from 0.2 to 0.5

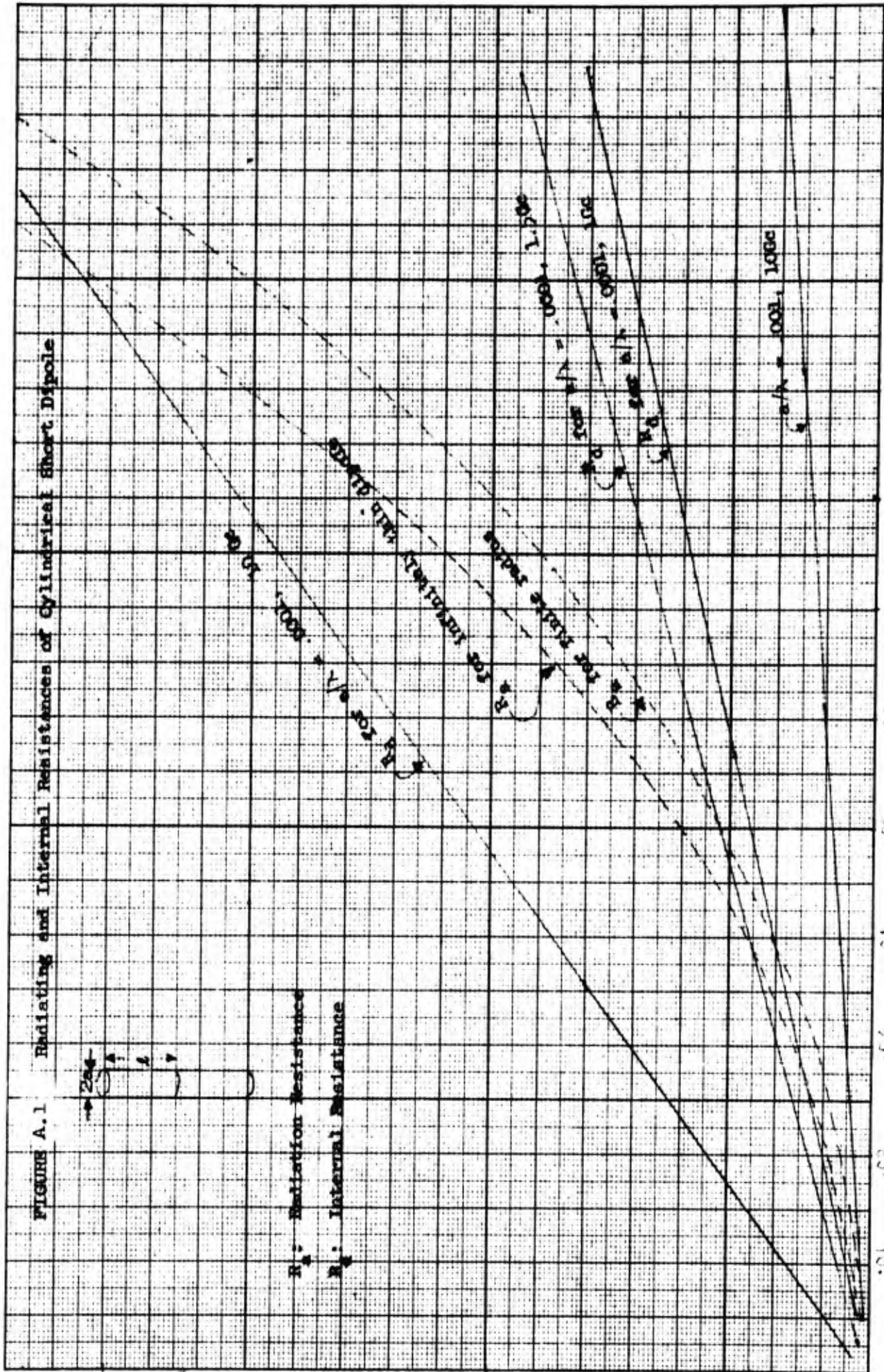


FIGURE 1.2 Input Resistances of the Center-Driven Dipole Antenna

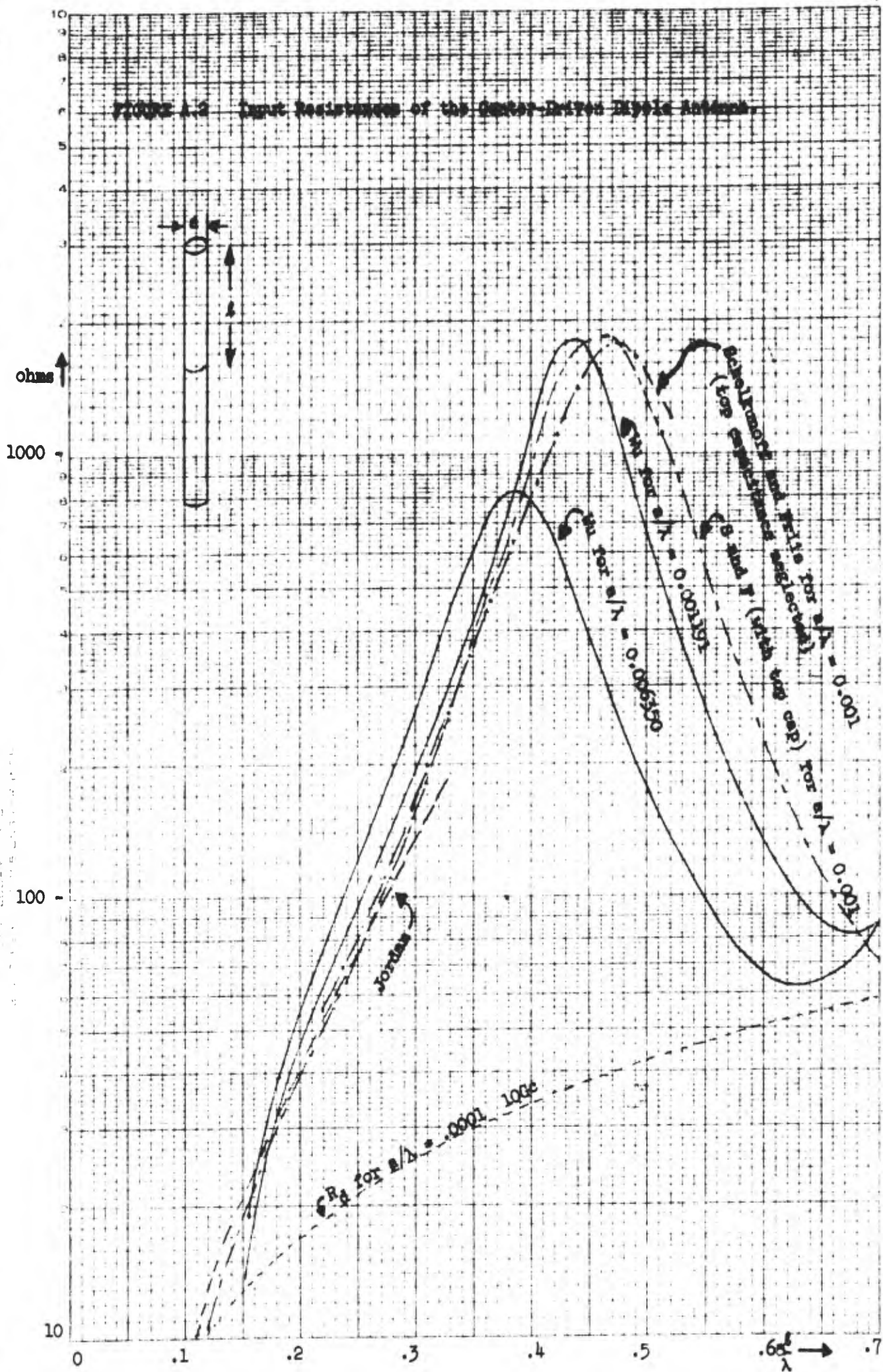
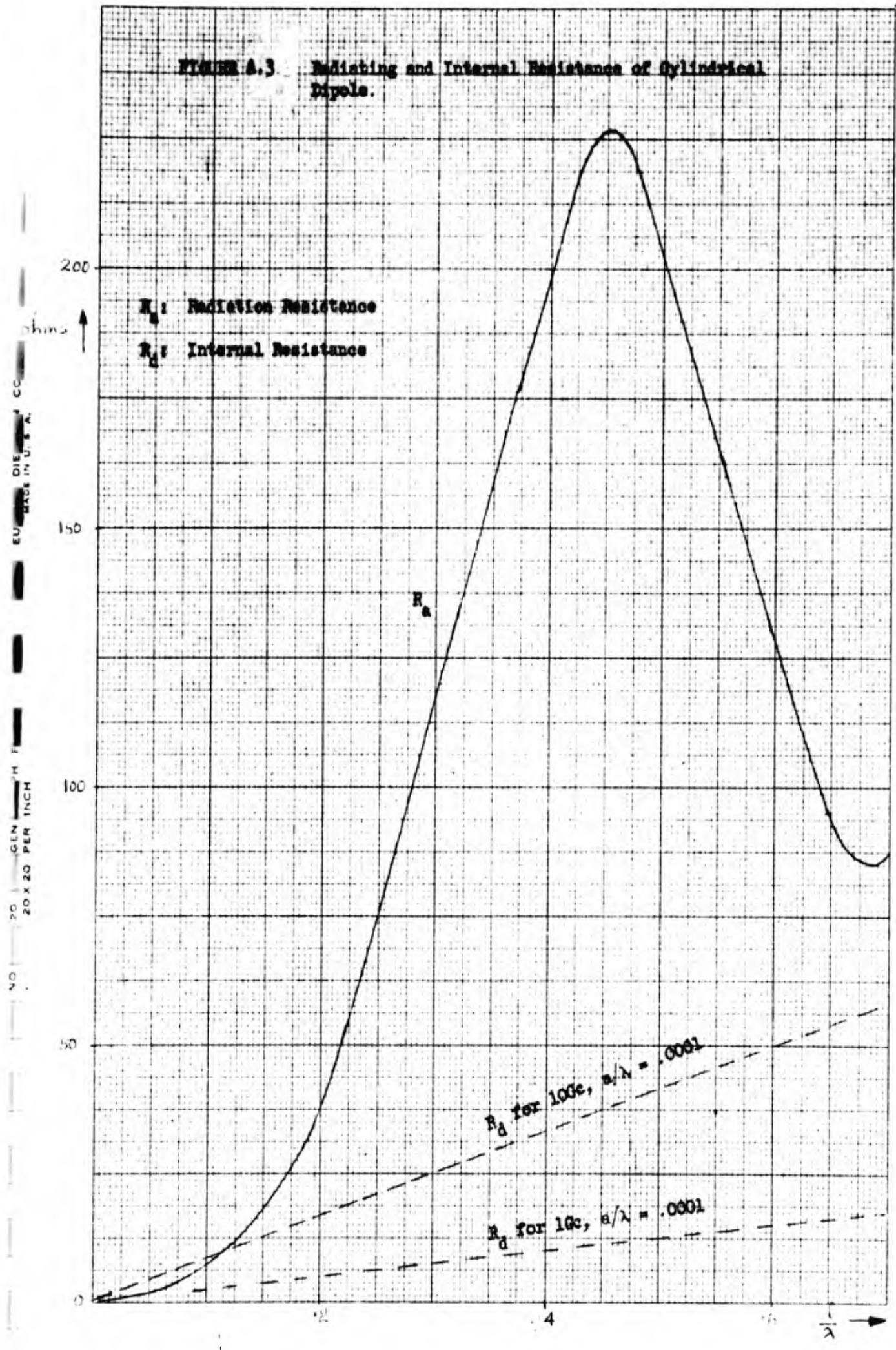


FIGURE A.3 Radiating and Internal Resistance of Cylindrical Dipoles.



20 GEN 20 PER INCH  
NO  
EU DIE MADE IN U.S.A.  
CC

(that is full-wave dipole). Also, it is noted that in fig. A.2 the curves obtained from reference 17 and Wu's paper<sup>22</sup> agree closely, and results given by Jordan<sup>15</sup> which describe the ideal case agree only when dipole length is about half-wave length.

#### A.4 Conclusion

When half-wave dipoles are used, the internal resistance can be neglected even at frequency of 10 Gc, but if the dipole is very short, internal resistances are considerable. If the dipole is not very thin (say,  $a/\lambda > 1/100$ ) internal resistance is negligible regardless of dipole length.

Appendix B

## INFLUENCE OF GAP ON DIPOLE INPUT IMPEDANCE

B.1 Introduction

In this section it is shown that the influence of finite gap on the input impedance of a dipole antenna which usually is assumed infinitesimal is not negligible. Besides a simple assumption of the sinusoidal current distribution of a dipole, there are three distinct theories; namely, Hallen-King theory based on  $\delta$ -gap model which leads to an integral equation, Stratton-Chu theory based on  $\delta$ -gap spheroidal model which can give a rigorous solution of Maxwell's equation and, finally, Schelkunoff's theory based on thin biconical model which is the only one that takes account of gap but neglects the end effect of cones.

There have been investigations of the influence of a dipole gap by Infeld<sup>6</sup> based on the Stratton-Chu theory and by King-Winternitz<sup>13</sup> based on the King-Middleton theory. Although the equation of the Stratton-Chu model is more rigorous than that of the King-Middleton model, the mathematical difficulty makes it impractical for numerical calculation.

The work of Infeld will be briefly summarized and the detailed discussion will be based on the work of King and Winternitz.

B.2 Influence of the Gap Width in a Spheroidal Model

We can characterize the points in space by the spheroidal coordinates<sup>16</sup>  $\zeta, \eta, \varphi$  with:

$$\zeta \geq 1, \quad |\eta| \leq 1, \quad 0 \leq \varphi \leq 2\pi$$



A spheroid is characterized by a constant coordinate  $\zeta = \zeta_0$ . The input admittance of a cylindrical dipole which has a length of  $2h$ , diameter of  $2a$  and gap width of  $2d$  is given by<sup>6</sup>

$$Y_d = \frac{-j k f}{60} (1 - \eta_0^2) \sum_{l=0}^{\infty} \frac{(\zeta_0^2 - 1) R_l^4(\zeta_0) S_l^1(\eta_0) \int_{-1}^{+1} (1 - \eta^2) g(\eta) S_l^1(\eta) d\eta}{\frac{d}{d\zeta_0} \left[ (\zeta_0^2 - 1) R_l^4(\zeta_0) \right] N_l} \text{ mho} \quad (\text{B.1})$$

where  $k = \omega(\mu_0 \epsilon_0)^{1/2}$  is wave number of surrounding medium which is air,  $f = \frac{L}{\zeta_0}$  is the distance between foci of the equivalent spheroid,

$$N_l = \int_{-1}^{+1} (1 - \eta^2) \left[ S_l^1(\eta) \right]^2 d\eta = 2 \sum_{n=0}^{\infty} \frac{A_n^2}{(n+1)(n+2)(2n+3)}$$

is the normalizing factor and  $g(\eta)$  is the function characterizing electric field at the gap with  $\int_{-1}^{+1} g(\eta) d\eta = 1$ . Constant coordinates  $\zeta_0$  and  $\eta_0$  are related to the dimensions of the dipole  $L$ ,  $a$  and  $d$  by

$$\frac{\zeta_0}{\sqrt{\zeta_0^2 - 1}} = \frac{L}{a}$$

$$\eta_0 = \frac{d}{L}$$

The spheroidal function of first kind  $S_l^1$  and the radial spheroidal function of fourth kind  $R_l^4$  are solutions of the general spheroidal wave equation<sup>4,5</sup>

$$\frac{d}{dz} \left[ (1 - z^2) \frac{dy}{dz} \right] + \left[ \lambda - c^2 z^2 - \frac{\mu^2}{1 - z^2} \right] y = 0 \quad (\text{B.2})$$

with  $c = fk$  and  $\mu = 0$ , and are given by<sup>6</sup>

$$S_\ell^1(\eta) = (\eta^2 - 1)^{-1/2} \sum_{n=0}^{\infty} A_n j^{n-\ell} \frac{n!}{(n+2)!} P_{n+1}^1(\eta) \quad (\text{B.3})$$

$$R_\ell^4(\zeta, c) = \frac{1}{c\zeta \sum_{n=0}^{\infty} A_n j^{n-\ell}} \sum_{n=0}^{\infty} A_n \left(\frac{\pi}{2c\zeta}\right)^{1/2} H_{n+\frac{3}{2}}^{(2)}(c\zeta) \quad (\text{B.4})$$

where  $P_n^1(\eta)$  is an associated Legendre function of the first kind and  $H_n^{(2)}(\zeta)$  is a Hankel function of the second kind. Since  $S_\ell^1(\eta) = 0$  if  $\ell$  is odd, eq. (B.1) becomes with  $g(\eta) = \delta(\eta)$

$$Y_d = -\frac{jkf}{60} (1-\eta_0^2) \sum_{m=0}^{\infty} \frac{(\zeta_0^2 - 1) R_{2m}^4(\zeta_0) S_{2m}^1(\eta_0) S_{2m}^1(0)}{\frac{d}{d\zeta_0} \left[ (\zeta_0^2 - 1) R_{2m}^4(\zeta_0) \right] N_{2m}} \quad (\text{B.5})$$

Equation (B.5) is identical with the input impedance of Stratton-Chu theory<sup>3</sup> if  $\eta_0 = 0$  or  $d = 0$ .

For large  $m$ , the eigen value of eq. (B.2)  $\lambda_{2m}$  is very large compared to  $f^2 k^2 \eta^2$  such that we can have following approximation for large  $m$

$$(1-\eta_0^2) S_{2m}^1(0) S_{2m}^1(\eta_0) = \frac{4m}{\pi} (1-\eta_0^2)^{1/2} \cos \left[ \left(2m + \frac{3}{2}\right) \eta_0 \right] \quad (\text{B.6})$$

$$N_{2m} = 2m \quad (\text{B.7})$$

and

$$\frac{(\zeta_o^2 - 1) R_{2m}^4(\zeta_o)}{\frac{d}{d\zeta_o} \left[ (\zeta_o^2 - 1) R_{2m}^4(\zeta_o) \right]} = \frac{1}{2m} (\zeta_o^2 - 1)^{1/2} \quad (\text{B.8})$$

Now for sufficiently large M

$$\begin{aligned} (1 - \eta_o^2) \sum_{m=M+1}^{\infty} \frac{(\zeta_o^2 - 1) R_{2m}^4(\zeta_o) S_{2m}^1(\eta_o) S_{2m}^1(o)}{\frac{d}{d\zeta_o} \left[ (\zeta_o^2 - 1) R_{2m}^4(\zeta_o) \right] N_{2m}} \\ = (\zeta_o^2 - 1)^{1/2} (1 - \eta_o^2)^{1/2} \sum_{m=M+1}^{\infty} \frac{\cos \left[ (2m + \frac{3}{2}) \eta_o \right]}{m} \end{aligned} \quad (\text{B.9})$$

Changing a summation to integral, eq. (B.9) becomes

$$(\zeta_o^2 - 1)^{1/2} (1 - \eta_o^2)^{1/2} \int_M^{\infty} \frac{\cos \left[ (2m + \frac{3}{2}) \eta_o \right]}{m} dm = (\zeta_o^2 - 1)^{1/2} (1 - \eta_o^2)^{1/2} \text{Ci} \left( \frac{M}{2} \eta_o \right) \quad (\text{B.10})$$

Substituting eq. (B.10) into eq. (B.5)

$$\begin{aligned} Y_d = - \frac{jfk}{60} (\zeta_o^2 - 1) (1 - \eta_o^2) \sum_{m=0}^M \frac{R_{2m}^4(\zeta_o) S_{2m}^1(\eta_o) S_{2m}^1(o)}{\frac{d}{d\zeta_o} \left[ (\zeta_o^2 - 1) R_{2m}^4(\zeta_o) \right] N_{2m}} \\ - \frac{jfk}{60\pi} (\zeta_o^2 - 1)^{1/2} (1 - \eta_o^2)^{1/2} \text{Ci} \left( \frac{M}{2} \eta_o \right) \end{aligned}$$

$$\begin{aligned}
&= -\frac{jak}{60} (\zeta_o^2 - 1)^{1/2} \left[ 1 - \left(\frac{d}{L}\right)^2 \right] \sum_{m=0}^M \frac{R_{2m}^4(\zeta_o) S_{2m}^1\left(\frac{d}{L}\right) S_{2m}^1(o)}{\frac{d}{d\zeta_o} \left[ (\zeta_o^2 - 1) R_{2m}^4(\zeta_o) \right] N_{2m}} \\
&- \frac{jak}{60\pi} \left[ 1 - \left(\frac{d}{L}\right)^2 \right]^{1/2} C_1 \left(\frac{M}{2L}\right) \tag{B.11}
\end{aligned}$$

when  $d$  approaches zero the first term of the equation approaches

$$-\frac{jak}{60} (\zeta_o^2 - 1)^{1/2} \sum_{m=0}^M \frac{R_{2m}^4(\zeta_o) \left[ S_{2m}^1(o) \right]^2}{\frac{d}{d\zeta_o} \left[ (\zeta_o^2 - 1) R_{2m}^4(\zeta_o) \right] N_{2m}}$$

and the second term tends to infinity like  $a \ln \left(\frac{d}{2L}\right)$ . Thus it shows that unless the dimension of the finite gap should be involved in the antenna theory the series for input admittance diverges. In other words, input impedance becomes zero for infinitesimal gap which is contrary to practice.

### B.3 Influence of the Gap Width on Hallén Model

Assuming  $\frac{2\pi a}{\lambda} \ll 1$  where  $\lambda$  is wavelength in surrounding medium and  $\frac{a}{L} \ll 1$ , three dimensional boundary value problems of cylindrical dipole as discussed in previous section can be reduced to one dimensional form and the integral equation for current distribution can be easily found by induced potential method. King-Middleton<sup>12</sup> solved this integral equation by method of successive approximation and derived following expression for the input impedance of a dipole with infinitesimal gap width

$$Z_0 = -j60\psi \frac{\sum_{n=0}^{\infty} F_n(L)/\psi^n}{\sum_{n=0}^{\infty} M_n(0)/\psi^n} \quad (\text{B.12})$$

where  $F_n(Z)$  and  $M_n(Z)$  are  $n^{\text{th}}$  order term of the approximating series.

The integral equation for the current distribution of a dipole antenna with the finite gap width  $2d$  differs from that of Hallens primarily in the limits of integrals and phase of approximating functions. Thus the input impedance of this dipole can be written as<sup>13</sup>

$$Z_d = -j60\psi \left\{ \frac{F_0(L-d) + F_0(d) \sum_{n=1}^{\infty} F_n^d(L)/\psi^n + G_0(d) \sum_{n=1}^{\infty} G_n^d(L)/\psi^n}{\sum_{n=0}^{\infty} M_n^d(d)/\psi^n} \right\} \quad (\text{B.13})$$

where superscript  $d$  indicates the difference of integral limits from the definition of that function. For a small quantity of  $d$  we can expand the functions in equation (B.13) in Maclaulin series in powers of  $2\pi\frac{d}{\lambda}$ . Hence, when  $2\pi\frac{d}{\lambda} \ll 1$  and  $\frac{d}{L} \ll 1$ , the input impedance is given by

$$Z_d = Z_0 / (1 - \epsilon) \quad (\text{B.14})$$

where correction factor  $\epsilon$  is given by

$$\epsilon = 2\pi \frac{d}{\lambda} \left\{ \frac{\sum_{n=0}^{\infty} G_n(L)/\psi^n}{\sum_{n=0}^{\infty} F_n(L)/\psi^n} + \frac{2}{\psi} \frac{e^{-j2\pi\frac{L}{\lambda}}}{2\pi\frac{L}{\lambda}} \left[ \frac{\sum_{n=0}^{\infty} \frac{F_n(0) - F_n(L)}{\psi^n}}{\sum_{n=0}^{\infty} F_n(L)/\psi^n} \right] \right. \\ \left. + \frac{2}{\psi} \frac{e^{-j2\pi\frac{L}{\lambda}}}{2\pi\frac{L}{\lambda}} \left[ \frac{\sum_{n=0}^{\infty} G_n(L)/\psi^n}{\sum_{n=0}^{\infty} M_n(0)/\psi^n} \right] \right\} \quad (\text{B.15})$$

Separating real and imaginary parts of eqs. (B.12), (B.13) and (B.15)

$$Z_o = R_o + j X_o$$

$$Z_d = R_d + j X_d$$

$$\epsilon = \epsilon'' - j \epsilon'$$

The input resistance and reactance of dipole antenna with gap become respectively

$$R_d = \frac{R_o(1 - \epsilon'') + X_o \epsilon'}{(1 - \epsilon'')^2 + (\epsilon')^2} \quad (\text{B.16})$$

$$X_d = \frac{X_o(1 - \epsilon'') - R_o \epsilon'}{(1 - \epsilon'')^2 + (\epsilon')^2} \quad (\text{B.17})$$

Now if we know the values of  $\psi$ , and function  $F_n(z)$ ,  $G_n(z)$ , and  $M_n(z)$ ,  $Z_d$  can be calculated.  $\psi$  is the approximation of a function

$$\psi(z) = \int_{-L}^L g(z, z') \frac{e^{-j2\pi \frac{R}{\lambda}}}{R} dz' \quad (\text{B.18})$$

where  $g(z, z')$  is the current distribution function which is unknown and

$R = \left[ (z - z')^2 + a^2 \right]^{1/2}$ . The best approximation of  $\psi$  is given by

$$\psi = 2 \ln \frac{2L}{a} \quad (\text{B.19})$$

which is same as the characteristic impedance of Schelkunoff's theory<sup>18</sup> if it is multiplied by  $\frac{1}{2\pi}$  times the characteristic impedance of the air. The functions  $F_0(z)$  and  $G_0(z)$  are given by

$$F_0(z) = \cos 2\pi \frac{z}{\lambda}, \quad G_0(z) = \sin 2\pi \left| \frac{z}{\lambda} \right| \quad (\text{B.20})$$

and higher order function is given by an identical recurrent relation

$$\begin{aligned} F_n(z) = & \left[ F_{n-1}(z) - F_{n-1}(L) \right] \int_{-L}^L g(z, z') e^{-j2\pi \frac{R}{\lambda}} dz' \\ & - \int_{-L}^L \left[ F_{n-1}(z) - F_{n-1}(L) \right] e^{-2\pi \frac{R}{\lambda}} dz' \\ & - \left[ F_{n-1}(z) - F_{n-1}(L) \right] \left[ \psi(z) - \psi \right] \end{aligned} \quad (\text{B.21})$$

In particular, assuming perfect conductor,  $F_1(z)$  and  $G_1(z)$  are given by<sup>11</sup>

$$\begin{aligned} F_1(z) = & - \left( \cos 2\pi \frac{z}{\lambda} - \cos 2\pi \frac{L}{\lambda} \right) \ln \left( 1 - \frac{z^2}{L^2} \right) \\ & + \frac{1}{2} \cos 2\pi \frac{z}{\lambda} \left[ \bar{C}i \left( 4\pi \frac{L+z}{\lambda} \right) + \bar{C}i \left( 4\pi \frac{L-z}{\lambda} \right) \right. \\ & \left. + j \text{Si} \left( 4\pi \frac{L+z}{\lambda} \right) + j \text{Si} \left( 4\pi \frac{L-z}{\lambda} \right) \right] \\ & - \frac{1}{2} \sin 2\pi \frac{z}{\lambda} \left[ \text{Si} \left( 4\pi \frac{L+z}{\lambda} \right) - \text{Si} \left( 4\pi \frac{L-z}{\lambda} \right) \right] \end{aligned}$$

$$\begin{aligned}
& - j \bar{C}i \left( 4\pi \frac{L+z}{\lambda} \right) + j \bar{C}i \left( 4\pi \frac{L-z}{\lambda} \right) \Big] \\
& - \cos 2\pi \frac{L}{\lambda} \left[ \bar{C}i \left( 2\pi \frac{L+z}{\lambda} \right) + \bar{C}i \left( 2\pi \frac{L-z}{\lambda} \right) \right. \\
& \left. + j Si \left( 2\pi \frac{L+z}{\lambda} \right) + j Si \left( 2\pi \frac{L-z}{\lambda} \right) \right] \tag{B.22}
\end{aligned}$$

$$\begin{aligned}
G_1(z) = & - \left( \sin 2\pi \left| \frac{z}{\lambda} \right| - \sin 2\pi \frac{L}{\lambda} \right) \ln \left( 1 - \frac{z^2}{L^2} \right) \\
& - \frac{1}{2} \cos 2\pi \frac{z}{\lambda} \left[ Si \left( 4\pi \frac{L+z}{\lambda} \right) + Si \left( 4\pi \frac{L-z}{\lambda} \right) \right. \\
& - 2 Si \left( 4\pi \left| \frac{z}{\lambda} \right| \right) - j \bar{C}i \left( 4\pi \frac{L+z}{\lambda} \right) \\
& \left. - j \bar{C}i \left( 4\pi \frac{L-z}{\lambda} \right) + 2j \bar{C}i \left( 4\pi \frac{z}{\lambda} \right) \right] \\
& - \frac{1}{2} \sin 2\pi \frac{z}{\lambda} \left[ \bar{C}i \left( 4\pi \frac{L+z}{\lambda} \right) - \bar{C}i \left( 4\pi \frac{L-z}{\lambda} \right) \right. \\
& \left. + j Si \left( 4\pi \frac{L+z}{\lambda} \right) - j Si \left( 4\pi \frac{L-z}{\lambda} \right) - 2j Si \left( 4\pi \frac{z}{\lambda} \right) \right] \\
& - \frac{1}{2} \sin 2\pi \left| \frac{z}{\lambda} \right| \left[ 4 \ln \frac{|z|}{L+|z|} - 2 \bar{C}i \left( 4\pi \frac{z}{\lambda} \right) \right] \\
& - \sin 2\pi \frac{L}{\lambda} \left[ \bar{C}i \left( 2\pi \frac{L+z}{\lambda} \right) + \bar{C}i \left( 2\pi \frac{L-z}{\lambda} \right) \right. \\
& \left. + j Si \left( 2\pi \frac{L+z}{\lambda} \right) + j Si \left( 2\pi \frac{L-z}{\lambda} \right) \right] \tag{B.23}
\end{aligned}$$



where

$$\bar{C}i(x) = \int_0^x \frac{1 - \cos \mu}{\mu} d\mu$$

$$Si(x) = \int_0^x \frac{\sin \mu}{\mu} d\mu$$

The function  $M_n(z)$  is given by the convolution of  $F_n(z)$  and  $G(z)$  as

$$\sum_n M_n(z) = \left[ \sum_n F_n(z) \right] \left[ \sum_n G_n(L) \right] - \left[ \sum_n F_n(L) \right] \left[ \sum_n G_n(z) \right] \quad (B.24)$$

In particular

$$M_0(z) = \cos 2\pi \frac{z}{\lambda} \sin 2\pi \frac{L}{\lambda} - \cos 2\pi \frac{L}{\lambda} \sin 2\pi \left| \frac{z}{\lambda} \right| \quad (B.25)$$

and

$$M_1(z) = F_1(z) \sin 2\pi \frac{L}{\lambda} - F_1(L) \sin 2\pi \left| \frac{z}{\lambda} \right|$$

$$+ G_1(L) \cos 2\pi \frac{z}{\lambda} - G_1(z) \cos 2\pi \frac{L}{\lambda} \quad (B.26)$$

A few tabulations of functions  $F_1(L)$ ,  $F_2(L)$ ,  $M_1(0)$  and  $M_2(0)$  can be found in literatures.<sup>2,10,12</sup>

#### B.4 Analysis and Conclusion

The first and second order approximation of  $\epsilon$  as a function  $\frac{L}{\lambda}$  has been shown by King-Winternitz<sup>13</sup> with  $\frac{d}{L}$  kept constant, but we are

interested in the change of input impedance as a function of the gap width with  $\frac{L}{\lambda}$  kept constant.

In fig. B.1, the input resistance for various sizes of dipoles are plotted as a function of  $\frac{d}{L}$  which are calculated using eq. (B.3). As shown in fig. B.1, the influence of dipole gap is negligible for a wide class of antenna thickness when the length is near the half wavelength and input reactance can be approximated by

$$\frac{X_d}{X_o} = \frac{\cot 2\pi \frac{L-d}{\lambda}}{\cot 2\pi \frac{L}{\lambda}} \quad (\text{B.27})$$

For a shorter dipole it can be seen that correction for the input resistance is necessary for which no simple formula is found, as well as input reactance for which eq. (B.27) is still a good approximation. We note that, however, the correction factor for the resistance  $\frac{R_d}{R_o}$  is not very sensitive for  $\frac{L}{\lambda}$  when  $\frac{d}{L}$  and  $\frac{a}{L}$  are kept constant.

To treat the dipole problem completely we have to include the influences of feeding lines, the unbalance of current on dipole<sup>8</sup> and others. Also we cannot neglect the problem of the change of the characteristic impedance of the feed line when connected to the dipole.<sup>9</sup> The above problems will have to be considered when short electric and magnetic dipoles are used in free space.

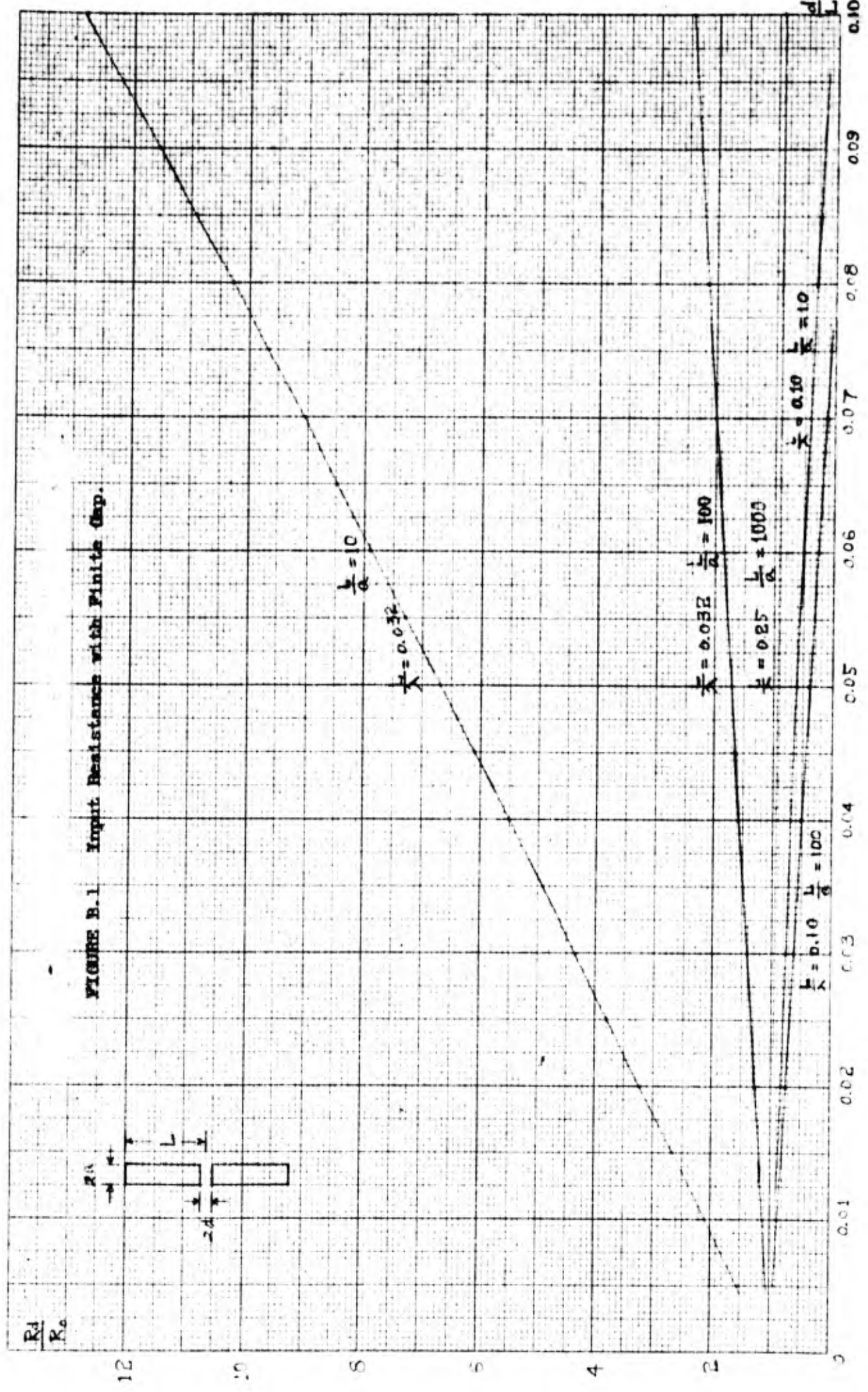


FIGURE B.1 Input Resistances with Finite Gap.

## REFERENCES

1. Bartfeld, R. A., et al, "Study of Methods of Improved Measurement for Electromagnetic Field Components," Final Report, Contract No. NBy-3200, Moore School Report No. 62-19, University of Pennsylvania, 31 July 1962.
2. Bouwkamp, C. J., "Concerning a New Transcendent, Its Tabulation and Application in Antenna Theory," Quart. of Appl. Math., vol. 5, pp. 394-402, 1947.
3. Chu, L. J. and J. A. Stratton, "Steady-State Solution of Electromagnetic Field Problems III," J. of Appl. Phys., vol. 12, pp. 241-248, 1941.
4. Erdélyi, A. (ed.), "Higher Transcendental Functions," vol. III, McGraw-Hill, New York, 1955.
5. Flammer, C., SPHEROIDAL WAVE FUNCTIONS, Stanford Univ. Press, Stanford, California, 1957.
6. Infeld, L., "The Influence of the Width of the Gap Upon the Theory of Antennas," Quart. of Appl. Math., vol. 5, pp. 113-132, 1947.
7. Iizuka, Keigo, "Photosensitive Probes," Electronics, January 25, 1963.
8. Iizuka, K. and R. W. P. King, "The Effect of an Unbalance on the Current Along a Dipole Antenna," IRE Trans., vol. AP-10, pp. 702-707, 1962.
9. Iizuka, K. and R. W. P. King, "Terminal-Zone Corrections for a Dipole Driven by a Two-Wire Line," J. of Research, N.B.S., vol. 66D, pp. 775-782, 1962.
10. King, R. and F. G. Blake, "The Self-Impedance of a Symmetrical Antenna," Proc. IRE, vol. 30, pp. 335-349, 1942.
11. King, R. and C. W. Harrison, "The Distribution of Current Along a Symmetrical Center-Driven Antenna," Proc. IRE, vol. 31, pp. 548-567, 1943.
12. King, R. W. P. and D. Middleton, "The Cylindrical Antenna: Current and Impedance," Quart. Appl. Math., vol. 3, pp. 302-335, 1946.
13. King, R. W. P. and T. W. Winternitz, "The Cylindrical Antenna with Gap," Quart. of Appl. Math., vol. 5, pp. 403-416, 1947.
14. Knowlton, A. E. (ed.) STANDARD HANDBOOK FOR ELECTRICAL ENGINEERS, 9th ed., McGraw-Hill, 1957.
15. Jordan, E. C., ELECTROMAGNETIC WAVES AND RADIATING SYSTEMS, Prentice-Hall, 1950.

16. Moon, P. and E. Spencer, FIELD THEORY FOR ENGINEERS, D. Van Nostrand, Princeton, N. J., 1961.
17. Ramo, S. and J. R. Whinnery, FIELDS AND WAVES IN MODERN RADIO, John Wiley, 1953.
18. Schelkunoff, S. A., "Theory of Antennas of Arbitrary Size and Shape," Proc. IRE, vol. 29, pp. 493-521, 1941.
19. Schelkunoff, S. A. and H. T. Friis, ANTENNAS THEORY AND PRACTICE, John Wiley, 1952.
20. Slater, J. C., MICROWAVE TRANSMISSION, McGraw-Hill.
21. Stratton, J. A., ELECTROMAGNETIC THEORY, McGraw-Hill, 1941.
22. Wu, T. T., "Theory of the Dipole Antenna and the Two-Wire Transmission Line," J. of Math. Phys., vol. 2, pp. 550-574, 1961.

**UNCLASSIFIED**

**UNCLASSIFIED**